RIGA TECHNICAL UNIVERSITY

Adham Ahmed Awad Elsayed Elmenshawy

INVESTIGATION OF PERFORMANCE IMPROVEMENT OF GAS TURBINE ENGINE BY OPTIMIZED DESIGN OF BLADE TURBINE COOLING CHANNELS

Summary of the Doctoral Thesis

RTU Press
Riga 2024

RIGA TECHNICAL UNIVERSITY
Faculty of Civil and Mechanical Engineering
Aeronautics, Space Engineering and Transport Institute

Adham Ahmed Awad Elsayed Elmenshawy

Doctoral Student of the Study Programme "Transport, Aviation Engineering"

INVESTIGATION OF PERFORMANCE IMPROVEMENT OF GAS TURBINE ENGINE BY OPTIMIZED DESIGN OF BLADE TURBINE COOLING CHANNELS

Summary of the Doctoral Thesis

Scientific supervisor

Associate Professor Dr. sc. ing.
Ali Arshad

RTU Press
Riga 2024

Elmenshawy, A. Investigation of performance improvement of gas turbine engine by optimized design of blade turbine cooling channels. Summary of the Doctoral Thesis. – Riga: RTU Press, 2024. – 50 p.

Published in accordance with the decision of the Promotion Council "RTU P–22" of 8 May, 2024, Minutes No. 04030-9.16.2/3.

Cover picture from www.pexels.com

https://doi.org/10.7250/9789934370946
ISBN 978-9934-37-094-6 (pdf)

DOCTORAL THESIS PROPOSED TO RIGA TECHNICAL UNIVERSITY FOR PROMOTION TO THE SCIENTIFIC DEGREE OF DOCTOR OF SCIENCE

To be granted the scientific degree of Doctor of Science (Ph. D.), the present Doctoral Thesis has been submitted for defence at the open meeting of RTU Promotion Council on August 30, 2024 at Zoom online meeting https://rtucloud1.zoom.us/j/94304241685.

OFFICIAL REVIEWERS

Dr. habil. sc. ing. Vitālijs Pavelko
Riga Technical University

Dr. sc. ing. Espen Oland
UiT The Arctic University of Norway, Norway

Dr. sc. ing. Iyad Alomar
Transport and Telecommunication Institute, Latvia

DECLARATION OF ACADEMIC INTEGRITY

I hereby declare that the Doctoral Thesis submitted for review to Riga Technical University for promotion to the scientific degree of Doctor of Science (Ph. D) is my own. I confirm that this Doctoral Thesis has not been submitted to any other university for promotion to a scientific degree.

Adham Ahmed Awad Elsayed Elmenshawy ……. (signature)

Date: ……

The Doctoral Thesis has been written in English. It consists of an Introduction, 4 chapters, Conclusions, 69 figures, 9 tables, and 2 appendices; the total number of pages is 145, including appendices. The Bibliography contains 106 titles.

CONTENTS

ABSTRACT

This Doctoral Thesis focuses on the critical challenge of cooling turbine blades in gas turbine engines, a component exposed to extreme temperatures and thermal stresses during operation. Predominantly, these blades experience intense heat due to fuel combustion in the engine's combustion chamber, necessitating efficient cooling methods to prevent overheating and failure. A key aspect of this research was the optimization of cooling channel designs within these blades. The channels that circulate coolant fluid are essential for maintaining blade temperatures within safe limits. The study emphasizes the design considerations crucial for effective cooling: accommodating the required flow rate with acceptable pressure drops and optimizing channel geometry for efficient heat transfer while minimizing profile losses. Material properties of the turbine blades, including thermal conductivity, heat capacity, and melting point, were also considered in the design phase of the cooling channels. An extensive statistical analysis was conducted on CF6 engines installed in B747 aircraft. This involved examining engine failures, performance tests, and borescope inspection (BI) reports under various operational conditions. The study provided a detailed examination of the exhaust gas temperature (EGT) margin and other engine parameters, offering insights into engine degradation and performance loss over time. This provided an important understanding to design cooling channels for the blade profile. In the next step, by employing computational and analytical methodologies, the study evaluated the cooling performance of the base model (original) of NASA's 3CX turbine blade. SolidWorks and ANSYS FLUENT were used in this analysis, supported by a MATLAB algorithm for data comparison with the reference experimental data. The research compared different cooling channel configurations, including U-bend, Net-shape, and Jet impingement types, specially designed for doctoral research. The designed channels revealed significant differences in drag forces and thermal performance based on their design features.

The findings demonstrate that channel geometry, specifically the hydraulic diameter, significantly influences cooling efficiency. The doctoral research reveals that jet impingement-type cooling channels showcased a notable improvement in cooling effectiveness for the turbine blade especially at the trailing edge, underlining the importance of channel design in enhancing turbine blade thermal performance. This study offers critical insights into turbine blade cooling, with implications for improving the operational efficiency and lifespan of gas turbine engines.

The Thesis has been written in English and contains 145 pages, 69 figures, 9 tables, and references to up to 106 literature sources.

The Topic Relevance

Turbine blades are critical components in gas turbine engines that are exposed to high temperatures and thermal stresses during operation. The blades are subjected to extreme heat generated by the combustion of fuel and air in the combustion chamber, which can cause the blades to overheat and fail if not properly managed. One common method of managing the high temperatures in turbine blades is to use cooling techniques. Cooling can be achieved by passing a coolant fluid, typically air or a mixture of air and fuel, through internal channels in the blade. The coolant fluid absorbs some of the heat generated by the combustion process and carries it away from the blade, which helps to keep the blade temperature within a safe operating range. However, the cooling process can also introduce new challenges in the design and operation of turbine blades. The design of the cooling channels must be optimized to ensure efficient heat transfer and minimize pressure losses. The coolant fluid flow rate, temperature, and distribution must also be carefully controlled to avoid hot spots and thermal gradients that can lead to thermal stresses and blade failure. In addition, the use of cooling channels can also affect the aerodynamic performance of the blade. The presence of cooling channels can increase the surface roughness of the blade, which can increase drag and reduce the overall efficiency of the engine. Therefore, the design of the cooling channels must also consider the aerodynamic performance of the blade and minimize any negative effects on the engine's overall efficiency.

Overall, the cooling of turbine blades is a critical aspect of gas turbine engine design and operation. Effective cooling techniques can help increase the service life of turbine blades and improve the performance and reliability of gas turbine engines.

The complex geometry of cooling channels makes them difficult and expensive to manufacture. Additionally, the small size of the channels can make them difficult to inspect and maintain. The researcher’s goal is to design a new geometry that can achieve better cooling configuration and is easily manufacturable.

The abovementioned problems determine the purpose of this work.

The Aim and Objectives of the Doctoral Thesis

The main aim of this study is to investigate the performance improvement of gas turbine engines by optimizing the design of blade turbine cooling channels. Turbine blade failures occur due to cooling problems and can have serious consequences on the performance and reliability of a gas turbine engine. Therefore, the set objectives were investigated based on these reasons.

Objectives

1. Design and optimization of special type of turbine blade cooling channels (U-bend type, net type, and jet impingement type) for improved heat transfer and cooling efficiency.
2. To investigate the CF6 engine failure due to heat effects causing damage to the turbine blade.

3. To carry out computational fluid dynamic (CFD) based analysis for investigation of heat transfer and flow phenomenon in turbine blade cooling channels.
4. To develop MATLAB codes to integrate with CFD software for temperature profiles and heat transfer.
5. To compare the thermal performance and aerodynamic characteristics of the three designed cooling channels.
6. To carry out heat transfer conjugation analysis under real turbine blade boundary conditions and compare with reference experiment results.
7. To compare the results achieved from the Doctoral Thesis with the experimental studies in literature.

The Scientific Novelty of the Thesis

1. Specially designed jet impingement type of turbine blade cooling channels that are optimized for the turbine blade for enhanced cooling.
2. A notable achievement is the detailed temperature profiling, especially at the trailing edge and suction side of turbine blades. This advancement provides critical insights into thermal stresses and performance, contributing to the prolonged durability and effectiveness of turbine systems.
3. Qualitative and quantitative analysis of the turbine blade cooling channels' thermal performance under various operational conditions.
4. Development of MATLAB algorithms that can be integrated with the CFD simulation environment and provide extremely accurate results for complex aerodynamic and heat transfer analysis within blade cooling channels.

Practical Significance of the Thesis

1. This research directly contributes to the turbine manufacturing industry. The proposed design of the cooling channels can be seamlessly integrated into existing turbine production processes. Adaptations required for this integration are minimal given the fact that modern additive manufacturing techniques can help this adaptation, offering a straightforward path towards enhancing turbine blade performance and extending their operational lifespan.
2. The optimized cooling channels significantly boost the cooling efficiency of turbine blades. By facilitating more effective heat dissipation, these designs can lead to a marked reduction in operational costs.
3. The cooling channel design showcased in this Thesis is highly scalable and versatile, adaptable to various turbine sizes and types. This universal applicability makes the

research valuable not just for large-scale power plants but also for smaller, localized energy generation applications.

4. The improved cooling efficiency also impacts maintenance needs and the durability of turbine blades. Enhanced cooling reduces thermal stress, thereby diminishing the frequency of maintenance and repairs.

Thesis Structure and Main Results

The Doctoral Thesis consists of an introduction, four chapters, and a conclusion. The introduction articulates the relevance and significance of the study. Further, the research aims, objectives, and scope – including both the subject and object of investigation were comprehensively outlined.

Chapter 1 exhaustively explore gas turbines, tracing their historical evolution and operational mechanics. This chapter also delves into advanced aspects such as the cooling processes of gas turbine engines and the latest research advances in turbine blade cooling technologies.

Chapter 2 is an additional but related study about engine performance that specifically focuses on empirical analysis, featuring a case study that examines the hot section failures of CF6 jet engines. This investigation is grounded in test reports gathered from various aircraft sources across different geographic regions. It underscores the utilization of real data obtained from engine performance tests and borescope inspection (BI) reports. This data serves as the foundation for scrutinizing the occurrences of failures within the CF6 sections, particularly the high-pressure turbine (HPT) section. The chapter also presents a statistical analysis of the behavior and deterioration of engine parameters. One notable aspect of this analysis is the monitoring of exhaust gas temperature (EGT) and EGT margin for CF6 engines operating in diverse climatic zones. This examination explores the correlation between take-off EGT and take-off thrust for CF6 engines utilized in B747-400 aircraft. It reveals variations in engine conditions based on the climatic zones in which these engines operate.

Chapter 3 employs computational fluid dynamics (CFD) to optimize and analyze the flow characteristics and heat transfer variations in different cooling channel types of turbine blades such as U-bend, net type, and jet impingement type cooling channel. The chapter also highlights the thermal and hydraulic characteristics of various cooling channel configurations at different Reynolds numbers (R_e). Key findings indicate that slimmer turning vanes are more effective in reducing drag and improving thermal performance. Net type cooling channels (Case 2) showed promising results in the N_{ua}/N_{u0} ratio at a R_e range of 10,000 to 50,000, while jet impingement type (Case 3) excelled in drag reduction at $R_e = 30{,}000$. Intriguingly, drag force remained constant across extensive Re ranges, suggesting a form of robustness in fluid dynamics. The results have significant implications for optimizing cooling efficiency in different operational conditions.

*Chapter 4 i*s dedicated to optimizing referenced data concerning cooling channels for turbine

blades, specifically through the implementation of jet impingement type cooling techniques. The chapter also encompasses the validation results obtained from comparing simulation and reference experimental data.

These results uncover a more pronounced temperature profile, particularly along the blade's edge regions, with a prominent effect on the blade's suction side. These disparities are a consequence of the inherent limitations of CFD simulations, as previously discussed. Notably, the temperature at the center of the blade registers as higher, with variations spanning from 10 K to 35 K. Nevertheless, the temperature contours observed in both investigations exhibit a consistent overall pattern, with the vane's trailing edge being the hottest point at 670 K. The comparison drawn between the CFD results of the current study and the NASA model results facilitates an analysis of the correlation between these two datasets and the accuracy of the current CFD model. The slight deviations between the two datasets can be attributed to the diverse assumptions and simplifications integrated into the current study's CFD model, as well as potential experimental inaccuracies in the NASA data.

Conclusions contain a summary of the executed work, section synthesizes the research findings, highlighting the most consequential outcomes and suggesting avenues for future scholarly inquiry.

Research Methodology

Computational fluid dynamics (CFD) is a powerful tool that can be used to design cooling configurations in gas turbine blades. CFD simulations can provide detailed predictions about the flow and heat transfer trends within the turbine blade, which can be used to optimize the cooling design and improve the thermal performance of the blade. The following methods were used in this research:

1. Literature survey: This involved gathering data from experimental tests of the gas turbine blade cooling configurations to use as a basis for the CFD simulation.
2. Modeling and design using SolidWorks: This involved creating a detailed 3D CAD model of the gas turbine blade and the cooling configuration using SolidWorks.
3. Initial domain configuration: This involved setting up the basic geometry and dimensions of the simulation domain, which includes the gas turbine blade and the surrounding fluid domain.
4. Mesh generation using ANSYS ICEM-CFD: This involved using ANSYS ICEM-CFD to generate a high-quality mesh that accurately represents the geometry of the gas turbine blade and the surrounding fluid domain.
5. Selection of heat transfer model: This involved reviewing and selecting the appropriate model, such as the conjugate heat transfer (CHT) model, to simulate heat transfer between the gas turbine blade and the surrounding fluid.

6. Selection of turbulence model: This involved reviewing and selecting the appropriate model, such as the SST k-omega or k-epsilon model, to use for simulating turbulence within the fluid domain.
7. Development of MATLAB algorithm: This involved developing a custom MATLAB code to perform the necessary calculations for the CFD simulation.
8. CFD simulation using ANSYS FLUENT: This involved using ANSYS FLUENT as the CFD solver to perform the actual simulation, using the selected heat transfer and turbulence models, as well as the custom MATLAB algorithm, and comparing the simulation results with the referenced experimental data.

The use of CFD simulations provides several advantages: lower costs and faster operation than the experimental methods, which allows for a more comprehensive analysis of the flow and heat transfer within the turbine blade. Additionally, CFD simulations can provide detailed information about the flow and heat transfer at different points within the blade, which can be used to design more efficient augmented heat transfer channels.

Therefore, the study employed the ANSYS FLUENT code as a CFD solver and ANSYS ICEM-CFD for mesh generation. ANSYS FLUENT is widely used commercial CFD software that can solve a wide range of fluid flow and heat transfer problems and generate high-quality meshes suitable for use in CFD simulations. Together, these tools can be used to perform detailed and accurate CFD simulations of the cooling configurations in a gas turbine blade.

Thesis Approbation and Publications

In the period of making the Thesis, seven publications have been published in international journals and conference proceedings.

1. A. A. A. E. Elmenshawy, and I. Alomar, and A. Arshad. "Optimization Turbine Blade Cooling by Applying Jet Impingement Cooling Channels", *Transport and Telecommunication Journal 24,* no. 3 (2023): 320–337. https://doi.org/10.2478/ttj-2023-0026.
2. A. A. A. E. Elmenshawy, and I. Alomar, A. Arshad, and A. Medvedevs. "Computational Fluid Dynamics Analysis of Flow Characteristics and Heat Transfer Variabilities in Multiple Turbine Blade Cooling Channels", *Transport and Telecommunication* Journal 25, no. 1 (2024): 77–96. https:// doi.org/10.2478/ttj-2024-0008
3. A. Arshad, P. Cong, A. A. A. E. Elmenshawy, and I. Blumbergs, “Design optimization for the weight reduction of 2-cylinder reciprocating compressor crankshaft,” Archive of Mechanical Engineering, vol. 68, no. 4, pp. 449–471, 2021, doi: 10.24425/ame.2021.139311.
4. P. Nagaraj, A. A. A. E. Elmenshawy, and I. Alomar, “VIBROACOUSTIC SOUNDPROOFING FOR HELICOPTER INTERIOR,” *Aviation journal, 27(1), 57–66*.2023, doi: 10.3846/aviation.2023.18629

5. A. A. A. E. Elmenshawy and I. Alomar, “Statistics and Investigation of CF6 Jet Engines Hot Section Failures,” Reliability and Statistics in Transportation and Communication. RelStat 2021. Lecture Notes in Networks and Systems, vol. 410. Springer, Cham2022, pp. 88–98. https://doi.org/10.1007/978-3-030-96196-1_9.
6. A. Arshad, A. J. Kallungal, and A. A. A. E. Elmenshawy, “Stability Analysis for a Concept Design of Vertical Take-off and Landing (VTOL) Unmanned Aerial Vehicle (UAV),” in 2021 International Conference on Military Technologies (ICMT), Jun. 2021, pp. 1–6. doi: 10.1109/ICMT52455.2021.9502764.
7. A. A. A. E. Elmenshawy and Y. A. H. Alshwaily, “Optimization of Propeller Performance for a Quadcopter Drone by Applying Aerodynamic Propeller-Ducts,” Reliability and Statistics in Transportation and Communication. RelStat 2021. Lecture Notes in Networks and Systems, vol. 410. Springer, 2022, pp. 186–197. doi: 10.1007/978-3-030-96196-1.

Author’s Contribution to Publications

The scientific publications were produced through a collaborative effort involving supervisor Professor Ali Arshad, co-authors, and consultants. The authors jointly planned and carried out the work on these publications. Table 1 provides a summary of the author's contribution to the research work included in the scientific publications.

CHAPTER 1. OVERVIEW OF GAS TURBINES AND COOLING TECHNOLOGY

1.1.Overview of Gas Turbine Engines

Gas turbine engines have a fascinating history spanning over a century. Initially theorized by John Barber in 1791 [1], the practical implementation of turbines powered by ongoing combustion became a reality in the early 20th century. French engineer Auguste Rateau was pivotal in this development, creating a basic gas turbine engine in 1903 [2]. This early version featured an axial compressor, a combustion chamber, and a turbine linked to a small electrical generator. Over time, these engines underwent significant enhancements in efficiency and capability. A crucial development occurred during World War II with the introduction of turbojet engines for aircraft propulsion. This marked a significant turning point, leading to widespread use in aviation. Post-war advancements brought about more sophisticated designs, advanced materials, and innovative cooling techniques. The fundamental components of a gas turbine engine include a compressor, combustion chamber, turbine, and exhaust outlet. The engine operates by continuously compressing air, mixing it with fuel, and igniting it in the combustion chamber. The generated hot gases drive the turbine, which then powers the compressor and any connected generators, with the exhaust gases finally being expelled through the nozzle. These engines operate by compressing air in the compressor, which is then mixed with fuel and ignited in the combustion chamber. The resulting hot gases expand and flow through the turbine, where their energy is harnessed to drive both the compressor and any attached generator [3]. Finally, the cooled exhaust gases are expelled through the exhaust nozzle. This process is a continuous cycle, allowing the engine to produce power efficiently.

1.2. Gas Turbine Engine Cooling Process

The secondary air system in a gas turbine engine plays a crucial role in cooling and sealing various engine components [4]. This system involves several key airflows:

1. **Compressor discharge air:** Air compressed in the compressor is channeled to the combustion chamber, where it cools vital components like combustor liners and turbine blades [5].
2. **Bleed air:** Some compressed air is diverted from the compressor discharge for cooling and sealing.
3. **Film cooling air:** Introduced at high velocity through special nozzles, this air forms a protective layer over hot components like turbine blades and vanes, shielding them from extreme heat and reducing failure risks [6].
4. **Seal air:** Directed to parts like rotor seals, bearing seals, and casing seals, this air prevents

leaks. Its pressure is carefully managed to balance effective sealing with minimal impact on engine performance [7].

5. **Cooling and sealing air flow control:** This involves regulating airflows using various valves, such as bleed and film cooling air valves, to control flow and pressure. These airflows are monitored for appropriate temperature and pressure distribution across engine components [8].

The secondary air system's design is essential for maintaining engine component coolness, preventing leaks, and ensuring overall engine performance and reliability. The design of the secondary air system is critical to the overall performance and reliability of the gas turbine engine [9].

1.3.Review of the Turbine Blade Cooling Research

Turbine blade cooling is a critical aspect of gas turbine engines. The blades in a turbine rotate at high speeds and are subject to high temperatures due to the combustion of fuel. The main objective of turbine blade cooling is to prevent overheating, which can lead to decreased efficiency and damage to the blades. The cooling is necessary to ensure that the turbine can operate at peak efficiency and to extend the service life of the blades [10].

With rising gas turbine inlet temperatures, now often reaching 1850 K, effective cooling is more critical than ever. This is because modern turbine blade alloys typically withstand temperatures only up to 1350 K. Hence, cooling protects the blades from thermal failure and maintains turbine efficiency [11].

Over the last five decades, significant research has been conducted to enhance turbine blade cooling, involving analytical, computational, and experimental methods. This research has led to a better understanding of the heat transfer processes in turbines and the development of more advanced cooling techniques. The evolution of turbine inlet temperatures since the 1960s reflects advancements in cooling and material technologies, indicating a trend toward more efficient and powerful gas turbines [12]. In conclusion, the advancement and refinement of turbine blade cooling technologies are essential for the ongoing development and efficiency of gas turbine engines. As these engines operate at increasingly higher temperatures, effective cooling systems are critical to prevent blade overheating and ensure longevity. The evolution of cooling methods, from film and transpiration to internal cooling, demonstrates a keen adaptation to the rising demands of modern turbine operations. The focus on research and development in this field underscores the importance of innovative cooling solutions in maintaining turbine efficiency and reliability in the face of escalating thermal challenges [13]. The future of gas turbine technology hinges on the continuous improvement of these cooling techniques, ensuring that turbines can meet the demands of higher efficiency and greater power output.

CHAPTER 2. STATISTICS AND INVESTIGATION OF FAILURES OF CF6 JET ENGINE'S HOT SECTION

The use of the available real data regarding the engine's performance tests and BI reports allowed to perform an investigation on the failures that occurred in the CF6 sections, mainly the high-pressure turbine (HPT) section, and provide statistical analysis of the engine parameters behavior and deterioration. EGT and EGT margin monitoring for CF6 engines in different zones allowed the authors to analyze the relationship between take-off EGT and take-off thrust for CF6 engines that are running in B747-400 aircraft operating in different climatic zones, and it shows that the condition of these engines is different. The author performed a comparison analysis between take-off EGTM for 17 CF6 engines with different life cycles based on BI. The author found that the most defective part in the engine is around the HPT section, especially in the stage one in the turbine blade and NGV. HPT BI showed cracks, burning spots, missing coating, and erosion in the stage one turbine blade. The combustor and HPT are the most sensitive parts in the engines, which can change performance because of any defect in both. Choosing qualitative materials with high properties will help to increase the life cycle and decrease the maintenance costs.

All above stated led to the following assumptions:

- Improving cooling channels in turbine blades and HPT nozzle will decrease fatigue and temperature. This requires a new cooling channel design.
- The combustor, especially its dome assembly and spectacle pate, requires improvements to make full control of the flame, which can prevent cracks that impact engine performance directly.
- To conjugate heat transfer for a turbine blade with cooling holes by optimizing several cooling channel designs.
- To increase turbine reliability, advanced prognosis and health monitoring systems must be implemented to anticipate the remaining life of turbine blades and discs, with an emphasis on fracture critical regions to avoid catastrophic failures.

CHAPTER 3. COMPUTATIONAL FLUID DYNAMICS ANALYSIS OF FLOW CHARACTERISTICS AND HEAT TRANSFER VARIABILITIES IN MULTIPLE TURBINE BLADE COOLING CHANNELS

3.1. Problem Description

This study addresses this gap by selecting a cooling channel with varying different cross-sections as its baseline model. Sourced from an actual gas turbine blade NASA C3X, this model incorporates protrusion structures on its surface [14]. The investigation includes a comprehensive analysis of flow dynamics, heat transfer, and resistance features for channels equipped with different designs of cooling channels. In the scope of this research, ANSYS FLUENT was employed for computational fluid dynamics (CFD) solving, while mesh creation was facilitated through ANSYS ICEM-CFD. The latter was specifically chosen for its capability to produce highly accurate and precise meshes compatible with CFD analyses. Collectively, these software tools enabled the execution of in-depth and precise CFD simulations focused on the cooling setups within the gas turbine blade (NASA C3X). MATLAB algorithms were used for comparison between reference experiment data and simulation results. Despite the critical nature of this issue, existing literature scarcely addresses cooling channels that incorporate factors like variable cross-sectional attributes and rotational effects. In this study, computational fluid dynamics (CFD) and numerical methodologies were employed to scrutinize the efficiency of three distinct cooling channel models characterized by variable cross-sectional features.

3.2. Methodology

The core goal of the present study is to engineer a state-of-the-art design for cooling channels in turbines, targeting a considerable augmentation in thermal efficiency and cooling efficacy coupled with a reduction in drag forces. Utilizing cutting-edge computational fluid dynamics (CFD) models and empirical analyses, the study aspires to establish a channel configuration that is versatile across an extensive range of Reynolds numbers and diverse flow regimes. A key focus of this investigation lies in an exhaustive examination of the fluid dynamics at various critical segments within the cooling channels, such as bends and junctions, with the intent to pinpoint zones requiring optimization. MATLAB algorithms are deployed for data processing, allowing for rigorous computational analysis and comparative evaluation based on experimental findings. Table 3 presents the three different designs of the cooling channel specifically designed for this study.

Table 1

Cooling Channel Designs

Case 1	U-bend cooling channel
Case 2	Net cooling channel
Case 3	Jet impingement-type cooling channel

3.2.1. U-Bend Optimization (Case 1)

The main goal of this design was to cover a wide area in the trailing edge. For the optimization, a 6.3 mm diameter of the original NASA C3X cooling hole was adopted, as in [14]. A modified 20 mm U-bend of the original channel with a bend angle of 129.5°, and symmetry were also applied as well with a full entire length of 76.2 mm as seen in Fig. 3.1 [14]. The focus here was to increase the angle in the U-bend, to help minimize pressure drop and drag. The pipe's geometrical design was created using ANSYS Workbench.

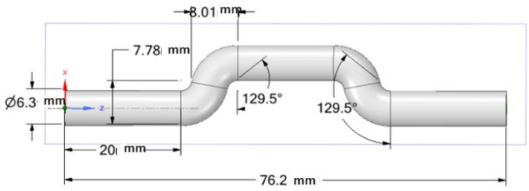

Fig. 3.1. Configuration of the U-bend model.

The cooling channel geometry and computational domain for starting meshing for this case were installed. Figure 3.2 presents the geometry before meshing and shows the name selected for this U-bend geometry.

Fig. 3.2. U-bend model flow domain.

The size and properties of a smooth channel with known reference experimental data were chosen to analyze the hydrodynamic and heat transfer characteristics through a straight channel. The size and features of the smooth channel from the reference experiment data investigation were employed as suggested by [15].

The mesh used in carrying out this model had the following properties: a bounding length of 14.44 mm, 6.3 mm, and 76.2 mm, and a total volume of 2,589 mm^2. One body was selected, and a mesh was created using CFD. Also, using an ICEM element size of 0.2 mm for this case provided more accuracy for the flow conditions.

Transport phenomena for momentum and other scalar quantities are most prominent in regions close to the wall, where solution variable gradients are larger. Therefore, in the Thesis, the inner layer was considered and was divided into three zones, each characterized by its respective non-dimensional distance, known as the wall Y^+ value. This value is analogous to the local Reynolds number. Specifically, the viscous sublayer corresponds to Y^+ values below 5, the buffer or transitional layer ranges from 5 to 30, and the fully turbulent layer is 30 and 60. For the purposes of this study, a viscous sublayer was assumed by selecting a Y^+ value of 1. Air serves as the fluid medium for this investigation, with a density of 1.229 kg/m^3 and a viscosity of 0.0000173 kg/m·s. The normal wall distance, denoted as Y, was calculated using a specific formula (3.1)

$$Y = \frac{Y^+ \nu}{u_\tau}, \tag{3.1}$$

where ν presents fluid viscosity, kg/m·s, and u_τ presents the friction velocity and can be calculated (3.2):

$$u_\tau = \sqrt{\frac{\tau_w}{\rho}}, \tag{3.2}$$

where $\boldsymbol{\rho}$ is the density, kg/m^3, and τ_w presents the wall shear stress, which can be calculated with (3.3):

$$\tau_w = 0.5\, C_f \rho\, u^2, \tag{3.3}$$

where C_f is the skin friction coefficient.

$$C_f = \frac{0.058}{R_e^{0.2}}, \tag{3.4}$$

where R_e is Reynolds number.

Equations (3.1)–(3.4) were used to calculate the normal distance to the wall, which is 0.00213 mm. Mesh inflation was done using the normal distance to the wall as the first layer thickness, with 10 layers and a growth rate of 1.35. The mesh contained 3,962,979 nodes, and 969,878 elements.

3.2.2. Optimization Design of Net Bend Cooling Channels (Case 2)

The core design principle aims to broaden the cooling coverage around the trailing edge of the turbine blade. Utilizing the original NASA C3X cooling channel diameter of 6.3 mm, as in [1], design features of three net channels were strategically positioned between every two existing channels [14], [16]. The design also integrates symmetry and has an overall length of 76.2 mm. Within this framework, two net-type channels each have a width of 5.2 mm, while the middle channel is slightly narrower – 4.2 mm, as illustrated in Fig. 3.6). The key advantage of this layout is the enhanced surface area available for cooling. To bring this design concept to fruition, computational modeling was performed using ANSYS Workbench.

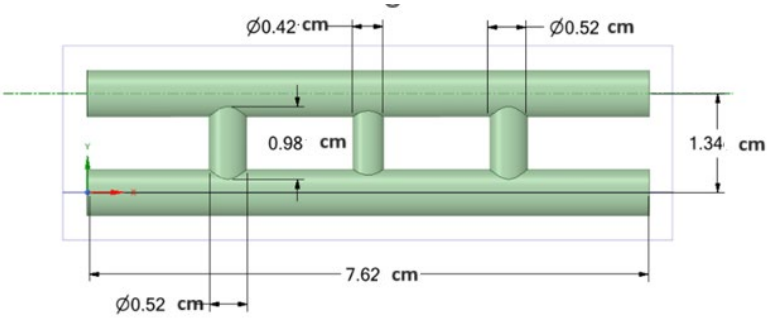

Fig. 3.3. Optimized model of net bend.

The size and properties of a smooth pipe with known reference experimental data were chosen to analyze the hydrodynamic and heat transfer characteristics through a straight pipe. The size and features of the smooth pipe were obtained from the experimental investigation in [14], which was employed in this study. The creation of the channel design used three-dimensional unstructured meshing. Mesh carried out for this model was done using the following properties: bounding length of 14.44 mm, 6.3 mm, and 76.2 mm and total volume of 2589 mm^2. The mesh was created using ANSYS ICEM. An element size of 0.5 mm for this case was chosen to provide more accuracy for the flow conditions. Equations (3.1)–(3.4), mentioned above, were used to calculate the normal distance to the wall, which gave a result of 0.00213 mm. Mesh inflation was also performed using normal distance to the wall as the thickness of the first layer, with ten layers and a growth rate of 1.2. The mesh contained 116291 nodes and 264,386 elements. Mesh independence criteria depicted the relationship between mesh element size and velocity across various mesh configurations. A trend of progressive increase in velocity with increasing mesh density can be seen till the mesh size of 264,386 elements, where the velocity is 161 m/s. After this point, the velocity curve becomes uniform, and the variations with respect to the mesh elements are insignificant. Therefore, after the suggested value from the mesh independence analysis, 264,386 elements were used for the CFD

analysis.

3.2.3. Optimization of Jet Impingement Cooling Channels (Case 3)

The focus of this study was on enhancing the cooling effectiveness of gas turbine components through an optimized jet impingement-type cooling channel. The study yielded promising outcomes, specifically an improved heat transfer coefficient and a reduced blade leading edge temperature, without causing a notable increase in pressure drop. This underscores the significance of precisely selecting jet impingement-type variables in cooling system designs for gas turbine elements. By retaining the mesh structure from the foundational model and incorporating insights from Glynn's research [17], it was confirmed that reducing the diameter of the channel jet nozzle can significantly enhance heat transfer. Additionally, this Doctoral Thesis adheres to Yamane's [18] guidelines on optimal nozzle height-to-diameter (H/DJ) ratios, which should range between 2 to 8. For this study, a jet diameter of 1.94 mm was selected, yielding a H/DJ ratio of 8, aligning well with Yamane's suggested parameters. Furthermore, the jet spacing to jet diameter (S/DJ) ratio was maintained between 4 and 8, with a selected jet spacing of 11.44 mm, resulting in an S/DJ ratio of 5.89. So, utilizing the ANSYS Workbench, the channel's geometrical design was created, and this optimized design was carried out with five jet channels. Figure 3.4 presents the configuration of jet impingement-type cooling channels.

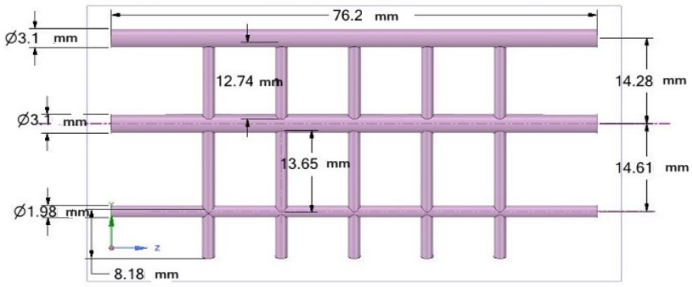

Fig. 3.4. Configuration of jet impingement cooling channels.

For the computational model in this study, the mesh was designed using CFX Solver. The mesh dimensions were set at 16.045 mm, 38.256 mm, and 76.2 mm with a total volume of 1871.9 mm^2, containing 243,212 nodes and 664,928 elements. A single domain was chosen for the analysis, and the element size was set at 4.338 mm to enhance flow condition accuracy.

Due to the dynamics of smaller scales of the channel and fluid momentum transport within them, the regions close to the wall are particularly active where the solution variable gradients are high. The mesh in these areas was divided into three distinct zones, each identified by its respective Y^+ value, a non-dimensional distance parameter related to the local Reynolds number. In this study, the

Y^+ values were categorized as follows: less than 5 for the viscous sublayer, between 5 and 30 for the buffer or transition zone, and 30 to 60 for the fully turbulent flow zone. For this analysis, a Y^+ value of 1 was selected, corresponding to the viscous sublayer near the wall. The fluid medium was chosen as air as the ideal gas, having a density of 1.229 kg/m^3 and a viscosity of 0.0000173 kg/m·s. Based on these parameters, the normal wall distance (Y) was computed using Eq. (3.1).

3.3. Numerical Method

The dynamics of fluid flow and heat transfer adhere to specific physical principles, and the mathematical representation of these fluid dynamics is derived by means of fundamental fluid flow governing equations. These complicated equations are typically resolved using numerical methods to investigate the underlying dynamics within fluid flow and heat transfer phenomena. This exploration yields valuable theoretical insights that can guide practical engineering applications. These governing Eqs. (3.5)–(3.8) are the mass equation, momentum equation, and energy equation, with the addition of the fluid state equation to ensure a comprehensive solution [19].

$$\frac{\partial \rho u_i}{\partial x_i} = 0 \tag{3.5}$$

$$\frac{\partial \rho u_i u_j}{\partial x_i} = \rho g_i + F_i - \frac{\partial P}{\partial x_i} + \frac{\partial}{\partial x_i} \cdot \left(2\mu S_{ij}\right) \tag{3.6}$$

$$\frac{\partial \rho u_i E_0}{\partial x_i} = \rho u_i F_i - \frac{\partial q_i}{\partial x_i} + \frac{\partial}{\partial x_j} \cdot \left(u_j T_{ij}\right) \tag{3.7}$$

$$\rho = f(\rho, T), \tag{3.8}$$

where

F_i – the body force, N;

P – pressure, N;

S_{ij} – the strain rate tensor, s^{-1};

E_0 – the total internal energy, J/kg;

T_{ij} – the surface force, Pa.

Equation (3.8) suggests that the density (ρ) of a substance is a function of its own density and temperature (T).

In the current investigation, the Reynolds-averaged Navier–Stokes (RANS) approach was implemented using a widely used finite-volume solver for our computations. Previous studies involving a three-pass channel structure equipped with turning vanes and ribs were explored in [15]. According to the studies in [15], the shear-stress transport (SST) k-ω turbulence model demonstrated a maximum deviation of 6.5 % from the experimental data. This was notably lower than the discrepancies found with realizable k-ω and RNG k-ω models, which showed errors of 19.3 % and

22.4 %, respectively. Therefore, this study opts to employ the SST k-ω model for more rigorous analysis.

For the evaluation of pressure drops, this research utilizes Eq. (3.10), which was derived from the Darcy–Weisbach equation [20]. The formula presumes the flow to be fully developed, in turbulent motion, and incompressible, with negligible variations in elevation or velocity along the conduit's length.

$$\Delta P = f\frac{L}{D}\frac{\rho U^2}{2g}, \tag{3.10}$$

where

ΔP – the pressure drop, Pa;

f – friction factor;

L – the length of the channel or pipe, mm;

D – the diameter of the channel, mm;

ρ – the density, kg/m^3;

U – the mean velocity of the fluid, m/s;

g – gravitational acceleration, m/s^2.

3.4. Parameter Definition

In the experimental setup by Wang [21], the central vane of the NACA C3X turbine blade received cooling via air circulation from the hub towards the root through a series of ten cylindrical channels. The blade material was constructed from ASTM 310 stainless steel. Wang's model replicated these conditions, defining the material properties of ASTM 310 stainless steel to include a specific heat capacity (Cp) of 502 J/kg·K and a density (ρ) of 8,030 kg/m³ [21], [22].

Based on the Wang's [21] study, in the Doctoral Thesis, the Reynolds Number (R_e) and the hydraulic diameter (D_C) for each cooling channel were derived from key parameters including fluid mass flow rate ($\dot{m}$), viscosity (μ), and coolant density (ρ). These calculations were carried out to ensure outlet pressure compatibility with NASA's C3X data by matching the inlet Reynolds number from 10,000 to 50,000. Reynolds number serves as a pivotal criterion for understanding flow behavior in each cooling channel. Turbulent flows, generally marked by higher Reynolds numbers, tend to favor elevated heat transfer rates but also lead to transitional flow regimes. These transitional phases present computational challenges, making it difficult to precisely model both flow behavior and heat transfer characteristics within the cooling system.

$$R_e = \frac{\frac{\dot{m}}{A}Dc}{\mu}, \tag{3.11}$$

where

ṁ – mass flow rate, kg/s;

μ – fluid viscosity, kg/m·s;

D_c – the cooling channel's hydraulic diameter, m;

A – the area, m^2.

Similarly, the Nusselt number was obtained by Eq. (3.12):

$$N_u = \frac{qD_C}{(T_w - T_f)\lambda}, \tag{3.12}$$

where

Tw – the wall temperature, K;

T_f – the average inlet temperature, K, based on mass flow;

λ – the thermal conductivity of the fluid, W/m·K;

q – the heat flux, W/m^2.

The Nusselt number (N_{u0}) was used to determine the (HTC) of each cooling channel [23].

$$N_{u0} = (0.023 P_r^{0.5} R_e^{0.8}), \tag{3.13}$$

where

Cr – correction coefficient;

P_r – Prandtl number;

R_e – Reynolds number.

Resistance factor (friction factor) f is represented as follows:

$$f = \frac{\Delta p D_C}{2\rho L u_{in}^2}, \tag{3.14}$$

where

L – length, m;

Δp – the pressure drop, Pa;

ρ – fluid density, kg/m^3;

u_{in} – fluid velocity, m/s.

The reference resistance factor f_0 [21] is calculated by (3.15):

$$f_0 = 0.507 R_e^{-0.3} . \tag{3.15}$$

Thermal performance (TP) provides a comprehensive assessment of the cooling channel characteristics and can be computed as follows:

$$TP = \left(\frac{N_{u_a}}{N_0}\right) \times \left(\frac{f}{f_0}\right)^{-1/3}, \tag{4.16}$$

where N_{ua} presents the average Nusselt number of all heating surfaces, including PS, SS, and tip wall surface.

Drag force is calculated by Eq. (4.17):

$$F_d = f \times \frac{L \times \rho \times U^2}{D_C} \times A, \tag{4.17}$$

where

L – length, mm;
ρ – fluid density, kg/m^3;
U – fluid velocity, m/s;
D_c – hydraulic diameter, mm;
f – friction factor.

3.5. Boundary Condition

The boundary condition taken for the experiment test has 4,311 codes, with 148 runs, as in [14], and a heat flux to the wall of 1,135 Watt/M2/K. The constant mass flow rate for the inlet is calculated by Reynolds number, and the inlet channel temperature of the cooling fluid is 298.15 K. Table 1 presents the boundary condition that the study used for simulation. The outlet pressure used for this study is 1 atm. The cooling fluid used for this study is ideal air gas.

3.6. Comparison of Results of Cooling Channels' Flow Characteristics

The comparison of the results obtained from the three designed cooling channels (U-bend, net type, and jet impingement type) is presented in this section. Nusselt number ratio is a very important and useful parameter for flow heat transfer. The importance of the Nusselt number ratio in this context lies in its ability to quantify the efficiency of heat transfer processes. A higher Nu_a/Nu_o ratio indicates a more effective convective heat transfer compared to conductive heat transfer. In practical applications, such as in cooling channels, this efficiency is crucial for maintaining optimal operating temperatures and ensuring the longevity and reliability of equipment. The observed variations in the Nusselt number ratio across different cases highlight the impact of design choices and operational parameters on heat transfer efficiency. The data reveals an initial decline in the Nusselt number ratio (N_a/N_{u0}) for all cases, followed by an increase as the Reynolds number (R_e) rises. Notably, the jet impingement cooling channel (Case 3) and the U-bend cooling channel type (Case 1) demonstrate more significant improvements compared to the net cooling channel (Case 2). The guide vane's thickness emerges as a critical factor influencing thermal exchange at the tip wall. As illustrated in Fig. 3.5, at a Reynolds number of 60,000, the jet impingement cooling channel type (Case 3) exhibits a significant increase of 25.3 % in the Nusselt number ratio (N_{ua}/N_{u0}). This enhancement is primarily due to the increased fluid acceleration in the outer region of the jet channels. Specifically, the significant increase in the N_{ua}/N_{u0} ratio for the jet impingement cooling channel underlines the effectiveness of this design in enhancing heat transfer, especially at higher Reynolds numbers.

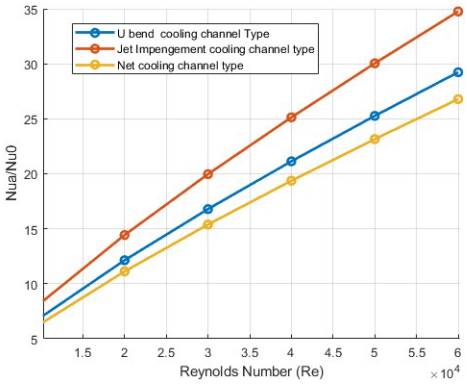

Fig.3.5. The variation ratio N_{ua}/N_{u0} with Reynolds number for U-bend cooling channel type, Jet impingement, and net cooling channel type.

The assessment of a channel's overall performance heavily relies on its frictional characteristics. Figure 3.6 illustrates the variations of f/f_0 with Reynolds number (R_e) for different cases. The data from the graph highlights that when Reynolds number (R_e) reaches 20,000, net cooling channels (Case 2) stand out with a remarkable 25.7 % reduction in drag. However, it is essential to note that excessively thick turning vanes can increase channel friction. This phenomenon occurs because as the thickness of the guide vanes increases, the flow area at the channel's corners decreases, leading to increased resistance due to the reduced cross-sectional area of the basin.

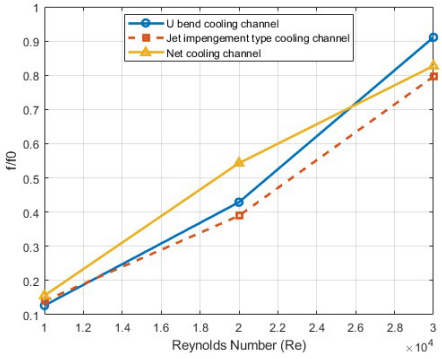

Fig. 3.6. The variation f/f_0 with Reynolds number for U-bend cooling channel type, Jet impingement, and net cooling channel type.

While at Re equal 30,000, the jet impingement type cooling channel (Case 3) reduces drag by 10.56 % compared to the net cooling channels (Case 2) and up to 20 % compared to U-bend cooling channels (Case 1).

The enhancement in the channel's thermal transfer efficiency often comes at the cost of

diminished frictional performance. The thermal performance (TP) metric offers a more holistic view by simultaneously accounting for both heat exchange and friction characteristics, thereby providing a well-rounded assessment of the channel's overall performance. Figure 3.7 illustrates how thermal performance (TP) varies with Reynolds number (R_e) across different channels. Initially, as R_e escalates, the TP for each channel experiences a decline, reaching its lowest point around R_e = 25,000. This phenomenon is largely attributed to minimal advancement in heat exchange levels and a noticeable uptick in channel friction at lower R_e values.

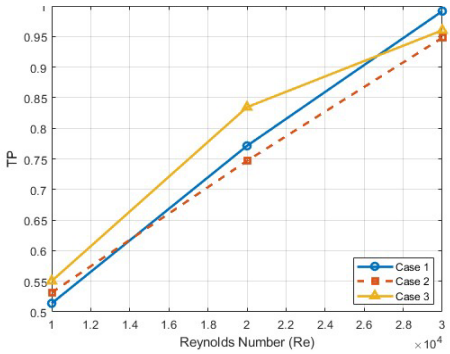

Fig. 3.7. The variation of TP with Reynolds number for different cooling channels.

Subsequently, as R_e continues to rise, heat transfer efficiency notably improves, leading to a corresponding increase in TP. Within the lower R_e range (10,000 to 30,000), when the Reynolds number (R_e) is at 10,000, the TP in net cooling channel (Case 2) sees an improvement of 3.5 %. However, an overly thick internal channel net can result in significant friction losses. In the R_e range of 20,000 to 30,000, the net cooling channel (Case 2) does not perform as well in terms of TP as in Case1. Jet impingement type (Case 3) showed better thermal performance at R_e 20,000 with 11.27 % than the U-bend cooling channel (Case 1). This leads to a gradual outperformance of jet impingement (Case 3) in TP compared to other channel configurations. Based on these observations, it can be projected that jet impingement-type cooling channels (Case 3) will offer the most balanced thermal performance when R_e exceeds. Figure 3.7 presents the variation of TP with Reynolds number for different cooling channels.

CHAPTER 4. OPTIMIZATION OF TURBINE BLADE COOLING CHANNELS BY APPLYING JET IMPINGEMENT-TYPE COOLING CHANNELS

4.1. Introduction

The goal is to optimize turbine blade cooling channels by applying the jet impingement method. The selection of experiment data for NASA 3CX turbine blade and 3D model using SolidWorks software and creating computational fluid dynamics (CFD) simulations were used to model the coolant flow and temperature distribution in the vane, while experimental testing can validate the CFD results and provide additional insights into the cooling system's performance. ANSYS FLUENT code was used as a CFD solver, and ANSYS ICEM-CFD was used for mesh generation. MATLAB algorithm is used for calculation using experiment data, and this was helpful for simulations. Heat transfer conjugation analysis bases SST shear stress analyses K-ω turbulent model. The results conclude that additional information is provided about the cooling channels and how they differ in the studies being compared. It then states that the cooling channels' hydraulic diameter decreases by a significant percentage, ranging from 49 % to 69 % as they are drawn to the trailing edge of the blade. This can have a significant impact on the heat transfer coefficients and the performance of the cooling system. The pressure side of the turbine blade is observed to follow the Hylton model, while the current study predicts a large over-anticipated heat transfer coefficient around the turbine blade head and on the bulk of the suction side. In terms of the average heat transfer coefficient, the two models differ by 23 %. The author found that the cooling effectiveness for the optimized jet impingement model is 0.4892 for the whole blade and compared it with the cooling effectiveness for the optimized jet impingement model, which is 0.6936. The results of the comparison between the base model and the optimized jet impingement model suggest that the optimized model has a significantly higher cooling effectiveness. The increase in cooling effectiveness of 29 % for the whole blade and 28.823 % for the trailing edge indicates that the optimized jet impingement design provides improved cooling performance. These results highlight the importance of considering optimized cooling designs for turbine blades to maintain efficient and safe operation.

4.2. Methodology

It is important to consider optimized cooling designs for turbine blades to keep efficient and safe operation. Computational fluid dynamics (CFD) is a powerful tool that can be used to design cooling configurations in gas turbine blades. CFD simulations can supply detailed predictions about the flow and heat transfer trends within the turbine blade, which can be used to optimize the cooling design and improve the thermal performance of the blade. The following methods were used in this research:

1. Collection of experiment data for NASA C3X using Hylton model data from experimental tests of the gas turbine blade cooling configuration to use as a basis for the CFD simulation.
2. Setting up the basic geometry and dimensions of the simulation domain, which includes the gas turbine blade and the surrounding fluid domain.
3. Select the the conjugate heat transfer (CHT) model to be used for simulating heat transfer between the gas turbine blade and the surrounding fluid.
4. Select the SST k-omega to be used for simulating turbulence within the fluid domain.
5. Modelling the design by creating a detailed 3D CAD model of the gas turbine blade and the cooling configuration using SolidWorks.
6. Mesh generation using ANSYS ICEM-CFD to generate a high-quality mesh that accurately is the geometry of the gas turbine blade and the surrounding fluid domain.
7. CFD simulation using ANSYS FLUENT as the CFD solver to perform the actual simulation, using the selected heat transfer and turbulence models, as well as the custom MATLAB code for numerical calculations.

4.3. Initial Base Model Configuration

NASA C3x Airfoil vane coordinates are given in Fig. 4.1, which presents cascade coordinate systems which are used to define the airfoil shape; the van was cooled by 10 radial cooling channels. Each hole configuration for the C3X vane is shown in Fig. 4.1. Solid works used to produce an outline of the spline's feature points were obtained by using the individual coordinates found in Hylton's experiment.

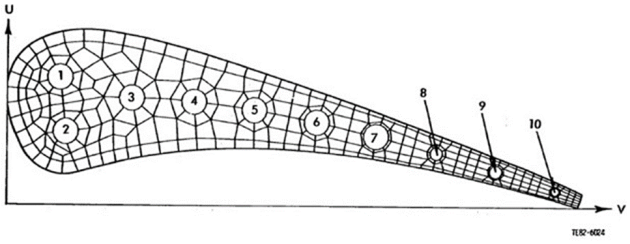

Hole No.	U--cm (in.)	V--cm (in.)	Diameter--cm (in.)	Cr
1	2.377 (0.936)	1.311 (0.516)	0.630 (0.248)	1.118
2	1.057 (0.416)	1.534 (0.604)	0.630 (0.248)	1.118
3	1.981 (0.780)	3.119 (1.228)	0.630 (0.248)	1.118
4	1.981 (0.780)	4.674 (1.840)	0.630 (0.248)	1.118
5	1.869 (0.736)	6.182 (2.434)	0.630 (0.248)	1.118
6	1.666 (0.656)	7.747 (3.050)	0.630 (0.248)	1.118
7	1.412 (0.556)	9.235 (3.636)	0.630 (0.248)	1.118
8	1.087 (0.428)	10.759 (4.236)	0.310 (0.122)	1.056
9	0.737 (0.290)	12.253 (4.824)	0.310 (0.122)	1.056
10	0.345 (0.136)	13.757 (5.416)	0.198 (0.078)	1.025

Fig. 4.1. Finite element grip structure for NASA c3x with cooling channel locations [14].

The 3D model was utilized in ANSYS fluent for running CHT (conjugate heat transfer) analysis

on both the original and optimized designs for the cooling channels. Figure 4.2 presents the original 3D design of the C3X turbine blade. Hylton incorporated the Cr (correction coefficient) constant into a modified Nusselt number expression that considered the effects of the thermal entrance region [14].

Hylton stated that the Cr constant is a function of P_r (Prandtl number), R_e (Reynolds number based on diameter), and X/D (distance from the leading edge normalized by diameter) [14]. The Cr (correction coefficient) constant from 1.03 to 1.12 was used for N_u (Nusselt number) calculation, and HTC (heat transfer coefficient) for 10 cooling channels [16]. The N_u and heat transfer coefficient were then compared with Hylton's, Wang's, and the baseline configuration data from the current study [6].

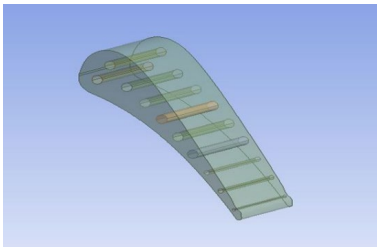

Fig. 4.2. Cooling of the base model turbine blade.

4.4. Mathematical Model

The governing equations used for this study are the continuity equation (Eq (4.1)), the time-averaged Navier–Stokes (NAS), and the energy equations for the turbulent model. In the present mathematical model, the momentum equations utilized in this investigation are represented by Eqs. (4.2)–(4.5) [24].

Continuity equation:

$$\frac{\partial \rho}{\partial t} + \frac{\partial (\rho u)}{\partial x} + \frac{\partial (\rho v)}{\partial y} + \frac{\partial (\rho w)}{\partial z} = 0, \tag{4.1}$$

where

u – the velocity components in X direction, m/s;

v – the velocity components in X direction, m/s;

w – the velocity components in X direction, m/s;

ρ_f – the fluid density, kg/m^3;

t – time, s.

Momentum equations:

$$\rho\left(u\frac{\partial u}{\partial x}+v\frac{\partial u}{\partial y}+\omega\frac{\partial u}{\partial z}\right)=-\frac{\partial p}{\partial x}+\mu_{nf}\left(\frac{\partial^2_u}{\partial x^2}+\frac{\partial^2_u}{\partial y^2}+\frac{\partial^2 u}{\partial z^2}\right) \quad (4.2)$$

$$\rho\left(u\frac{\partial v}{\partial x}+v\frac{\partial v}{\partial y}+\omega\frac{\partial u}{\partial z}\right)=-\frac{\partial p}{\partial y}+\mu_{nf}\left(\frac{\partial^2_v}{\partial x^2}+\frac{\partial^2_v}{\partial y^2}+\frac{\partial^2 v}{\partial z^2}\right) \quad (4.3)$$

$$\rho\left(u\frac{\partial w}{\partial x}+v\frac{\partial w}{\partial y}+\omega\frac{\partial w}{\partial z}\right)=-\frac{\partial p}{\partial z}+\mu_{nf}\left(\frac{\partial^2_w}{\partial x^2}+\frac{\partial^2_w}{\partial y^2}+\frac{\partial^2 w}{\partial z^2}\right), \quad (4.4)$$

where

u – the velocity components in X direction, m/s;
v – the velocity components in X direction, m/s;
w – the velocity components in X direction, m/s;
μ – dynamic viscosity, kg/m·s;
P – pressure, Pa;
ρ – the fluid density, kg/m^3.

The energy derivation relation equations have been used [19].

$$\frac{\partial}{\partial x_i}\left(\rho u_i\ C_pT-k\frac{\partial T}{\partial x_j}\right)=u_i\frac{\partial p}{\partial x_i}\mu\left(\frac{\partial u_i}{\partial x_j}+\frac{\partial u_j}{\partial x\ddot{\imath}}\right)-\frac{2}{3}\ \mu\frac{\partial u_k}{\partial x_k}\delta_{ij}, \quad (4.\ 5)$$

where

$\frac{\partial}{\partial x_i}$ – the partial derivative with respect to the spatial coordinates;
ρ_f – the fluid density, kg/m3;
u_i – the velocity components in the *i*-th direction, m/s;
C_p – the specific heat at constant pressure, J/(kg·K);
T – temperature, K;
k – the thermal conductivity, W/m·K;
μ – dynamic viscosity, kg/m·s;
δ_{ij} – the Kronecker delta, which is 1 when $i = j$ and 0 if otherwise.

Turbulent flow model

The Wang-RSM model is a type of Reynolds stress model (RSM) and differs from other commonly used models for turbulence, such as the shear stress transport (SST) k-ω model, the standard k-ω model, the k-kl-ω model, and the k-ε model [22]. The SST k-ω model is a turbulence model that uses two equations and combines the benefits of the k-ω and k-ε models. Specifically, it utilizes the k-ω model close to walls and the k-ε model in the outer region of the boundary layer. The SST k-ω model is popular because of its ability to accurately predict a wide range of flow types and geometries while being robust. In this study, the author used the SST k- ω model, which helps to intend for turbulent flows with large-scale anisotropy, especially cooling channels. Equations (4.6) and (4.7) present the SST k-ω model [22].

$$\rho\left(\frac{\partial k}{\partial t} + u \cdot \nabla k\right) = \nabla \cdot \left[\left(\mu + \frac{\mu t}{\sigma k}\right)\nabla k\right] + P_k - \beta^* \rho k\omega + S, \quad (4.6)$$

where

k – turbulence kinetic energy;

μt – turbulent viscosity and the turbulence production term, kg/m·s;

β^*–the model constant;

ω – the specific dissipation rate, m^2/s^3;

σk – the turbulent Prandtl number for k;

S – the source term resulting from buoyancy and external forces;

μ – dynamic viscosity, kg/m·s;

P_k– the production term of k.

$$\rho\left(\frac{\partial \omega}{\partial t} + u \cdot \nabla \omega\right) = \nabla \cdot \left[\left(\mu t + \frac{\mu t}{\sigma_\omega}\right)\nabla \omega\right] + \beta\rho\left(\frac{\omega}{k}\right) * \left(\frac{P_k}{\omega}\right) - \beta^* \beta \rho \omega^2 + S_t, \quad (4.7)$$

where

ω – specific dissipation rate of k;

μ_t – turbulent viscosity, kg/m·s;

σ_ω – the turbulent Prandtl number for ω;

S_t – the source term due to buoyancy and external forces.

To calculate turbulent viscosity for this model, the author used Eq. (4.8):

$$\mu t = \frac{\rho C \mu k^2}{\omega}, \quad (4.8)$$

where

$C\mu$ – the constant, typically set to 0.09;

k – the turbulence kinetic energy, J/kg;

ω – the specific dissipation rate of k;

ρ – density, kg/m^3.

For pressure drop calculation, the author used Eq. (4.9), which is based on the Darcy–Weisbach equation [20]. This equation assumes that the flow is fully developed and turbulent and that there are no significant changes in elevation or velocity along the length of the channel.

$$\Delta P = f \frac{L}{D} \frac{\rho U^2}{2g}, \quad (4.9)$$

where

ΔP – the pressure drop, Pa;

f – the friction factor;

L – the length of the channel or pipe, m;

D – the diameter of the channel, m;

ρ – the density, kg/m^3;

U – the mean velocity of the fluid, m/s;

g – gravitational acceleration, m/s^2.

4.5. Heat Transfer Conjugation

Heat transfer conjugation includes three different physical heat transfers: external area sides, flow, heat transfer, internal cooling passages, and ducts inside the blade structure. In the conjugate method, combined outer and inner flow and heat transfer with the blade line. The temperature distribution of the blade is determined by analyzing these three sections. The result in external flow and heat transfer simulation boundary conditions are used for the calculation of metal wires. Internal boundary conditions for line calculations are defined by simulation of internal heat and fluid flow coolant channel. As mentioned in the previous section, 3D simulation of heat transfer by internal cooling blade complex cooling passages is time-consuming. In Wang's experiment, the center vane of the C3X transonic turbine was cooled by air flowing from the hub to the deck through ten circular flow channels. The blade material was specified as ASTM type 310 stainless steel. The experiment was modeled by Wang to ASTM 310 stainless steel with a specific heat, C_p = 502 J·K/kg, density, ρ = 8,030 kg/m^3, and thermal conductivity varying by temperature displayed by Eq. (10) [22], [25]:

$$Kss = 0.0155T + 9.9105 \text{ (W·K/m)}. \tag{4.10}$$

In the simulation, Sutherland's formula was employed to characterize viscosity and thermal conductivity. It is important to note that specific heat capacity, dynamic viscosity (represented as μ), and thermal conductivity (denoted as $\boldsymbol{k_{fg}}$) are all influenced by temperature. Consequently, these properties exhibit temperature-dependent behavior, and their respective values can be determined using formulas that are sensitive to temperature variations. This information is encapsulated in Eqs. (4.11)–(4.12) [26].

$$\mu(T) = \mu_0 \left(\frac{T}{T_0}\right)^{\frac{3}{2}} \times \frac{T_0+s}{T+s} \tag{4.11}$$

$$k_{fg}(T) = \lambda_0 \left(\frac{T}{T_0}\right)^{3/2} * \frac{T_0+S}{T+S}, \tag{4.12}$$

where

μ_0 – reference dynamic viscosity, Pa·s;

T_0 – reference temperature, K;

λ_0 – reference thermal conductivity, W/m·K;

S – Sutherland's constant.

The dynamic viscosity of the fluid, denoted as μ(T), is a key parameter in fluid dynamics, representing the fluid's resistance to shear or flow. It is calculated based on a reference dynamic viscosity, μ$_0$, which is set at 1.7894 × 10^{-5} Pa·s. This reference value corresponds to a specific reference temperature, T_0, established at 273.11 K. The temperature of the fluid, represented by T, plays a crucial role in determining the actual dynamic viscosity. Additionally, the equation

incorporates Sutherland's constant, denoted as S, which is a fluid-specific value and integral to the calculation. For the fluid in question, Sutherland's constant is determined to be 110.56. This constant is pivotal in adjusting the viscosity calculation to accommodate variations in temperature, ensuring accuracy in the fluid's behavior analysis under different thermal conditions. The thermal conductivity of the fluid, represented as $k_{fg}(T)$, is a fundamental parameter in the study of fluid dynamics, characterizing the rate at which heat is conducted through the fluid. This property is particularly crucial in applications involving heat transfer and energy exchange.

To accurately assess $k_{fg}(T)$, we establish a reference point known as λ_0, the reference thermal conductivity. This reference value is essential for comparative and baseline measurements. For the purposes of our analysis, λ_0 is set at 0.0261 W/m·K, offering a standardized measure against which the thermal conductivity of the fluid at varying temperatures can be evaluated.

The Reynolds number and hydraulic diameter were calculated for each cooling hole based on the fluid mass flow rate (ṁ), hydraulic diameter for the cooling channel (D_C), the viscosity of the coolant (μ), and the density of the coolant (ρ). The calculation was carried out to match the outlet pressure, which required the inlet Reynolds number (R_e) to match the data from NASA C3X. Reynolds number is a crucial factor in determining the flow behavior within each cooling channel. If the flow is turbulent, it is more likely to result in maximum heat transfer, but this type of flow also creates transitional flow regimes. When the flow is in a transitional regime, it can create challenges for simulations to accurately predict the flow behavior and heat transfer within the cooling system. The coolant inlet R_e number was calculated based on the (D_C) hydraulic diameter of each channel using Eq. (4.13) displayed below. The equation is used to determine the characteristics of each of the individual cooling passages.

$$R_e = \frac{\frac{\dot{m}}{A} D_c}{\mu}, \tag{4.13}$$

where

ṁ – mass flow rate, kg/s;

μ – fluid viscosity, kg/m·s;

D_c – the cooling channel's hydraulic diameter, m;

A – the area, m^2.

The 3D dimensional calculation domain for the conjugation of heat transfer around the NASA C3X plate was modeled only once to validate the heat transfer coefficient distribution around the plate and to perform calculations. The 3D domain for the conjugate heat transfer simulation is depicted in Fig. 4.3.

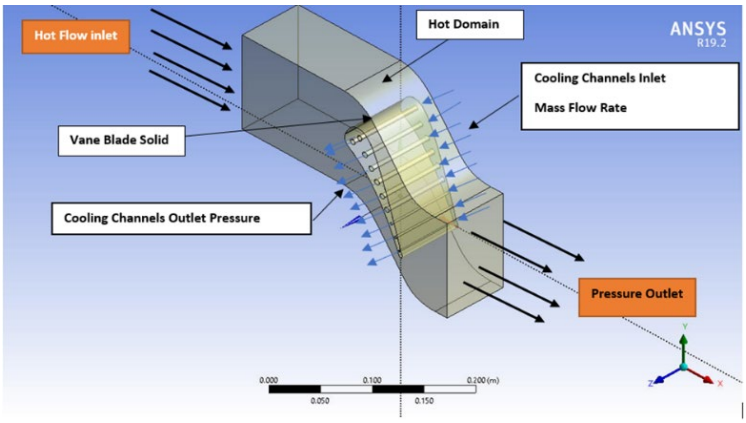

Fig. 4.3. The 3D domain of turbine blade with cooling channels.

The use of computational fluid dynamics (CFD) and various meshing techniques, such as prism layer for meshing, polyhedral mesh, and cylinder mesh generalized, were utilized in the current study to design and analyze the cooling configurations in a gas turbine blade. The goal was to achieve the greatest cooling efficacy while minimizing the impact on the thermodynamic system, as measured by the heat transfer coefficient (HTC). The study also compared the results to data from previous studies by Hylton and Wang. The Nusselt number equation was used to determine the HTC of each cooling channel.

$$N_{u0} = Cr\left(0.022 p_r^{0.5} R_e^{0,8}\right), \tag{4.14}$$

where

Cr – correction coefficient;

P_r – Prandtl number;

R_e – Reynolds number.

The average heat transfer coefficient (HTC) is an important parameter in the design of cooling systems for gas turbine blades. It is used to quantify the amount of heat transferred from the metal to the coolant and is typically expressed in units of W/m^2·K. The HTC is determined by several factors, including the fluid properties, flow conditions, and geometrical parameters of the cooling system. The Nusselt number (N_u) equation, which relates the HTC to the fluid properties and flow conditions, is commonly used to calculate the HTC. The correction coefficient (C_r), Prandtl number (P_r), and Reynolds number (R_e) are key parameters in the Nu equation and are used to account for the effects of fluid properties, flow conditions, and geometrical parameters on the HTC. The HTC values calculated using the N_u equation can then be used to compare the cooling performance of different cooling configurations and to optimize the design of the cooling system for improved thermal

performance. To be able to determine the Nusselt number N_u, this flow made numerous assumptions (N_u). The convective heat transfer coefficient was then calculated using the N_u. The heat flow around the vane was steady and uniform by the author. The author then assumes that the Hylton experimental temperature data was subjected to a set temperature boundary condition. For the heat transfer calculations reported, the author then used a constant thermal load [22], [25]. Finally, the heat transfer coefficient will vary depending on the cooling channel parameters, such as diameter and Reynolds number. Various features of the coolant had to be predicted to accommodate the varied heat transfer coefficient per cooling channel. Assume, for example, that the inlet flow temperature is uniform and constant, as specified in [14], [16], [22], [25].

The number is defined above, and the Prandtl number is as follows in Eq. (4.15) [16].

$$P_r = \frac{c_p \mu}{k_{fg}}, \tag{4.15}$$

where

C_p – the coolant's specific heat capacity, J/kg·K;

μ – fluid viscosity, kg/m·s;

k_{fg} – thermal conductivity represented by Sutherland's Law, as illustrated above, W/m·K.

The heat transfer coefficient was then determined using the N_u, as shown in Eq. (4.16):

$$h = \frac{k_{fg} N_u}{Dc}, \tag{4.16}$$

where $\boldsymbol{k_{fg}}$is thermal conductivity, and Dc is the cooling channel's hydraulic diameter. The heat transfer coefficient can be lowered to Eq. (4.17) by combining Eq. (4.11), (1.15), and (4.16) [22], [25]:

$$h = 0.02424 \cdot C(\lambda, \dot{m}, \mu) D_C^{-1.8}. \tag{4.17}$$

In Eq. (4.18), C represents the coefficient associated with a cooling channel and is assumed to be a constant cause of the coolant assumptions mentioned previously.

$$C(\lambda, \dot{m}, \mu) = \lambda \cdot (\frac{\dot{m}}{\mu})^{0.8} \tag{4.18}$$

The C.S.(Control Surface) calculated the HTC using Newton's law of cooling. The heat transfer coefficient is calculated by Ansys using the Eq. (4.19):

$$h = \frac{(q'' \, conduction \, (a))}{[|a| \, T_S - T_w)]}, \tag{4.19}$$

where

T_S – the standard temperature, K;

T_w – the boundary temperature, K.

T_S is the standard temperature, where it was supposed to be the average volume, and mean bulk temperature for the fluid of the individual channel, T_w is the boundary temperature, for the wall and

$\frac{(q'' \, conduction \, (a))}{[|a|]}$ is the vector field's heat flux boundary conduction. The heat flux at the boundary considers the impact of both molecular and turbulent diffusion effects on the fluid's boundaries. This analysis was applied to assist in forecasting the average heat transfer statistics of each cooling channel, and the findings on the average heat transfer coefficient (HTC) of the cooling channel are presented in the results section.

NASA C3x turbine blade boundary condition taken from C3X cascade test conditions: code 4311, run 148 [14].

4.6. Base Model Meshing

Achieving mesh independence is an important step in CFD simulations, particularly when performing a conjugate heat transfer (CHT) analysis. Mesh independence means that the solution obtained from the simulation should be relatively insensitive to the mesh density and should converge to the same solution regardless of the number of mesh elements or the mesh geometry. To attain mesh independence, several meshing parameters were employed, including the prism layer mesh, polyhedral mesh, and generalized cylinder mesh. The prism layer mesh is applied to enhance the accuracy of the flow model solution by generating prismatic cells that are orthogonal close to wall surfaces and boundaries, using the core volume mesh. This approach can help enhance the simulation accuracy near the walls, where the flow exhibits high viscosity. Polyhedral meshes and generalized cylinder meshes are also effective in generating high-quality meshes that can be employed in CHT analysis. These mesh types provide a balanced solution to the challenges of mesh generation by creating an extruded mesh along portions that resemble generic cylinders. This approach can be useful for simulating intricate geometries or areas with high curvature. Finally, the use of the control volume option in Ansys ICEM allows the author to coarsen or refine a specific portion of the mesh to more precise values. This can be useful for refining the mesh in regions where the flow or heat transfer is particularly important or where the solution is expected to be highly sensitive to the mesh density. Mesh was generated using ICME Ansys, using tetrahedrons method, and maximum growth rate 1.2, selecting curvature normal angle 18°. The created mesh has 3,184,243 elements, and 682,571 nodes. Inflation is used with a first layer thickness of 0.0021 mm and an overall number of layers is 10; this is very important for CHT accuracy. Momentum and other scalar transports are most active in near-wall regions where there are larger gradients in the solution variables [27]. The inner layer for this case made from three zones with corresponding wall Y^+ , which is a non-dimensional distance, which is the same as the local Reynolds number. Y^+ can be described as a viscous sublayer Y^+ less than 5, Y^+ for buffer layer or blinding region is between 5 and 30, and for fully turbulent Y^+ between 30 and 60. For this case, the assumed viscous sublayer is $Y^+ = 1$.

4.7. Optimized Model Configuration

In the current study, the optimized jet impingement-type configuration was designed with the objective of increasing cooling effectiveness while maintaining similar pressure drops compared to

the base model. The results demonstrated that the optimized jet impingement-type configuration successfully improved cooling effectiveness by enhancing the heat transfer coefficient and reducing the temperature at the blade's leading edge. This underscores the significance of considering jet impingement parameters in the design of cooling systems for gas turbine components. Utilizing the same meshing approach as the base model and drawing from Glynn's research [17], it was confirmed that heat transfer can be enhanced by reducing the jet nozzle diameter. It is essential to carefully determine jet impingement parameters, such as the position and diameter of the jet nozzle. According to Yamane's experiments, the *H*/*DJ* Ratio should fall between 2 and 8, where *H* represents the distance between the nozzles and *DJ* is the jet diameter. By selecting a jet diameter of 1.94 mm, the *H*/*DJ* ratio reached 8, aligning with the recommended ratio based on Yamane's experiment [18]. Additionally, the jet spacing, expressed as the *S*/*DJ* ratio, should be within the range of 4 to 8. The determination was made to set the jet spacing at 11.44 mm, resulting in an *S*/*DJ* ratio of 5.89. Figure 4.4 presents the flow domain and optimized turbine blade cooling channel (jet impingement type).

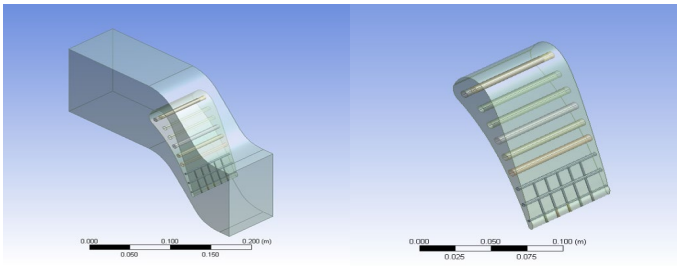

(a) **(b)**

Fig. 4.4. Flow domain and optimized turbine blade cooling channel model: (a) hot domain configuration; (b) optimized turbine blade cooling channels.

Meshing was carried out using Ansys ICEM, and the same base model mesh configuration CFD simulation was carried out using the same boundary condition used on the base model.

4.8. Results

The present study involves a comparison of outcomes derived from various cooling configurations through the utilization of CFD simulations, employing Helton's NASA model and Wang's CFD [25]. This comparative analysis will be structured into three distinct sections, each dedicated to specific cooling configurations and their notable attributes. Additionally, the study will showcase the data collected and evaluated within its scope, encompassing contour plots illustrating temperature, pressure, and heat transfer calculations. This comprehensive comparison aims to pinpoint the most efficient cooling configuration while offering valuable insights for enhancing the performance of gas turbine blades and vanes.

4.8.1. Configuration of Base Model

In this study, graphical representations are presented to compare the mean gauge pressure, mean temperature, and heat transfer coefficient data obtained from Hylton's dataset with the data generated from the current base model. This comparison was achieved by aligning similar span vs. axial cord positions (x vs. l) with the sensor locations in the Hylton dataset, enabling the display of corresponding means at those positions [14]. Figure 4.5 displays the normalized C3X vane span coordinate. To standardize the data, the parameter $p/p*$ was calculated using Hylton's inlet conditions, which were conducted at a nominal gas-stream total temperature of 811 K. Figure 4.6 presents the mean gauge pressure data for the base model. This comparison serves to evaluate the accuracy of the current CFD model in comparison to the NASA model, and it enables an assessment of the correlation between the two datasets, thereby validating the results obtained in the current study. It is worth noting that Hylton's NASA data is widely recognized as a benchmark in the aeronautical industry, and any alignment between the current study's data and the NASA data enhances the credibility of the current study's results when compared to the C3X vane data.

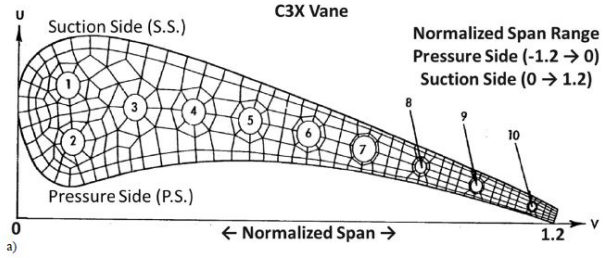

Fig. 4.5. Normalized C3X span coordinate [14].

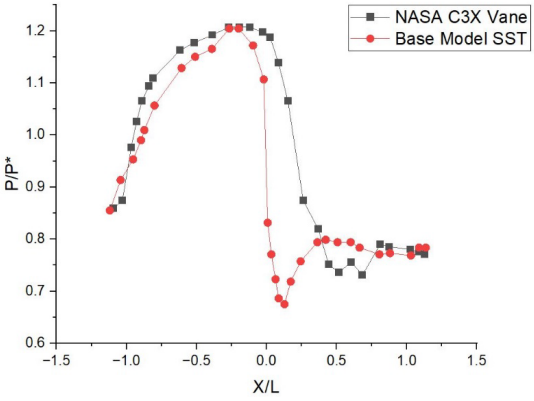

Fig. 4.6. Base model's mean gauge pressure data compared with C3X vane data.

In the current study, Fig. 4.7 displays a comparison of temperature distribution between the study's data and Helton's NASA C3X model experiment data, which is normalized between t/811 to mid-span [14]. Meanwhile, Fig. 4.8 exhibits the local heat transfer coefficient distribution over the turbine blade mid-span. Analyzing the temperature distribution comparison allows for an evaluation of the correlation between the two data sets and the accuracy of the current CFD model. The vane's pressure side follows the Hylton trend, but the current study predicts an overestimated heat transfer coefficient around the vane head and the majority of the suction side. The two models have a 23 % difference in average *h*, which may be due to the various assumptions and simplifications in the current CFD model and potential experimental errors in the NASA data. However, the difference falls within an acceptable range, and the study's results are trustworthy and precise.

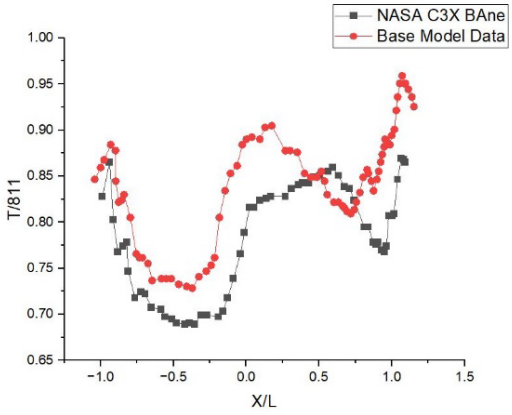

Fig. 4.7. Base model temperature comparison with NASA C3X experimental data.

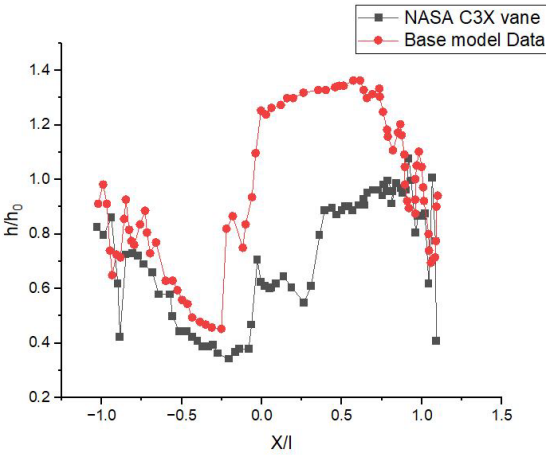

Fig. 4.8. Average heat transfer coefficient comparison.

In Fig. 4.9 in this current study, the temperature distribution in Kelvin (K) is depicted from the top view of the basic blade model configuration. Both models exhibit a similar temperature profile with slight variations. However, the current model indicates a higher temperature profile, particularly towards the edge regions, which is most pronounced on the blade's suction side. These distinctions arise from the limitations inherent in CFD simulations, as previously discussed. Notably, the temperature at the blade's center is elevated, ranging from 10 K to 35 K. Nevertheless, the temperature contours in both investigations follow the same overall pattern, with the vane's trailing edge displaying the highest temperature, exceeding 670 K. By comparing the CFD results of the current study with those of the NASA model, as well as with the studies by Wang and Rossman, we can assess the degree of correlation between the two datasets and evaluate the accuracy of the current CFD model. This can assess the correlation between the two datasets and the accuracy of the current CFD model [28]. Figure 4.9 provides visual representations of the temperature contours generated in the current study's baseline for the three configurations. The minor discrepancies observed between the two sets of data can be attributed to the diverse assumptions and simplifications incorporated into the CFD model of the current study, as well as the potential presence of experimental errors in the NASA dataset [14], [16], [22], [25].

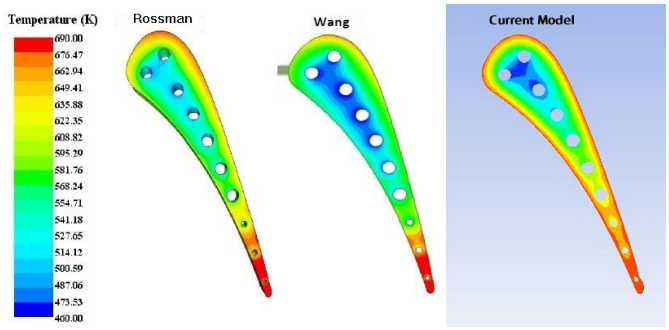

Fig. 4.9. Comparison of base model mean temperature data.

4.8.2. Trailing Edge Focus

In this section of the study, recent data is employed to underscore the vital importance of adopting a jet impingement-type configuration to enhance the cooling of turbine blade trailing edges. This configuration yields significantly lower temperatures compared to the baseline case, which exhibits a temperature range of 633 K to 685 K, as depicted in Fig. 4.10. The comparison clearly illustrates the advantages of employing a jet impingement-type cooling setup, particularly in dissipating heat at the vane's trailing edge, where temperatures reach their peak. This information holds crucial implications for the design and optimization of cooling systems for turbine blades and vanes, as it highlights the potential for a triple impingement cooling configuration to greatly improve the performance and efficiency of gas turbine engines.

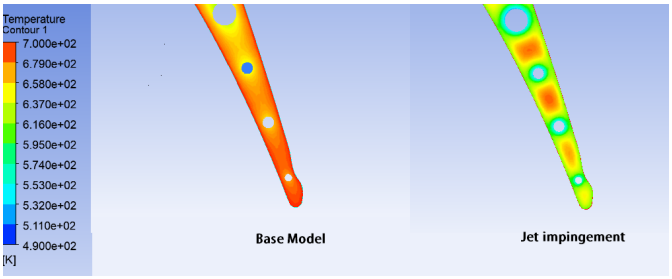

Fig. 4.10. Trailing edge temperature comparison between NASA base model and optimized model.

In the current study, the network impingement arrangement demonstrates even cooler temperatures than the base model. It ranges from 545 K to 598 K, which is 3.1 % to 3.9 % cooler, and the vane itself is 14.7 % to 20 % cooler compared to the original NASA C3X vane. Notably, the largest temperature drop is observed at the trailing edge's tip, as depicted in Fig 4.11. In the base model, the vane's tip reaches a temperature of 700 K, while its trailing edge tip registers at 652.75 K. This represents a substantial 18.3 % reduction in temperature compared to the baseline and network cooling jet impingement type. This underscores the effectiveness of the jet impingement-type cooling configuration in dissipating heat from the vane's hottest region, the trailing edge, leading to enhanced performance and efficiency in gas turbine engines.

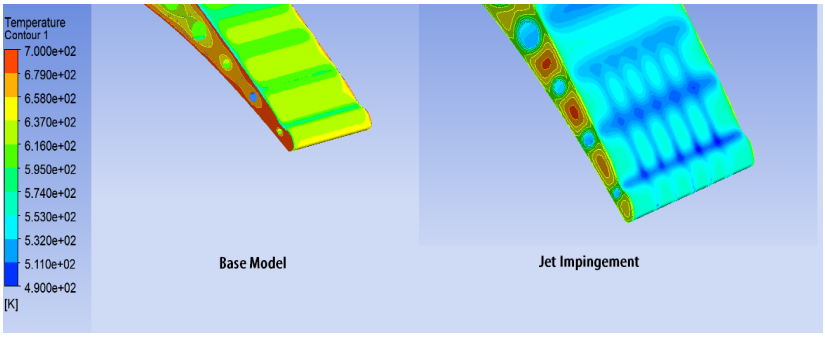

Fig. 4.11. 3D Trailing edge temperature comparison between NASA base model and optimized model.

The jet impingement-type configuration proves to be an efficient approach for lowering the temperature at the trailing edge tip of a turbine vane, a critical area prone to failure under high temperatures. The noteworthy 32.20 % reduction in temperature at the trailing edge tip when compared to the baseline configuration, along with an 18.95 % decrease compared to the NASA model configuration, signifies a substantial enhancement in the turbine's thermal performance. This improvement has the potential to significantly prolong the lifespan of the turbine components.

.

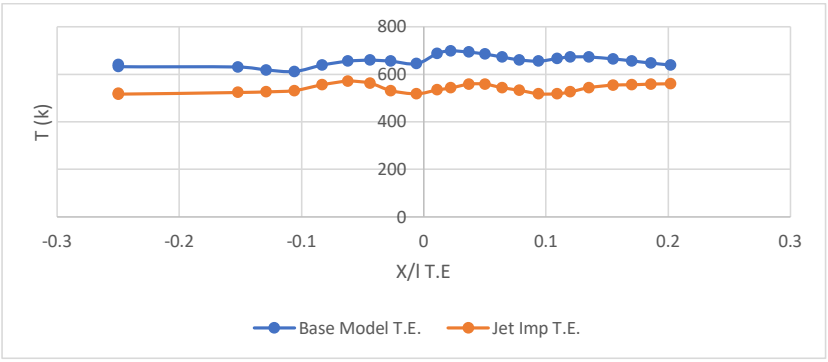

Fig. 4.12. Trailing edge temperature comparison between NASA base model and optimized model.

Figure 4.12 illustrates that among the three configurations examined in the study, the jet impingement-type configuration was most effective in lowering the temperature across the vane. The temperature distribution in this configuration was notably cooler compared to the other two, indicating its superiority as a cooling method. Such efficient cooling is crucial for mitigating issues like degradation, corrosion, and vane failure, which typically arise under high-temperature conditions.

4.8.3. Conjugate Heat Transfer

This text segment outlines an upcoming comparison between the calculated and measured average heat transfer coefficients for each cooling channel. The specific equations slated for use in these calculations are designated as Eqs. (4.14)–(4.20). These equations are presumably formulated to compute the heat transfer coefficient employing various methods or models.

The purpose of this comparison is multifaceted. Primarily, it aims to assess the precision and dependability of the calculated results in comparison to experimental measurements. This evaluation serves to verify the effectiveness and accuracy of the equations employed. Additionally, comparison is instrumental in identifying any variances or inconsistencies between the calculated and measured values. Such a comparative analysis is crucial, as it may lead to adjustments or enhancements in the equations or models currently used for calculations. These refinements are essential for improving the accuracy and reliability of future calculations, ensuring they more closely align with experimental observations and real-world data.

Figure 4.13 presents a graphical comparison of the average heat transfer coefficients (HTC) as calculated in different studies. The accompanying caption elucidates the graph's contents. It is noted that the HTC in the current study's computational fluid dynamics (CFD) baseline case is slightly under-predicted for the first eight cooling channels. However, this under-prediction becomes more noticeable near the trailing edge of the vane. This observation aligns with the principle that HTC varies with the hydraulic diameter of the cooling channel, a concept grounded in the fundamentals

of heat transfer and fluid dynamics.

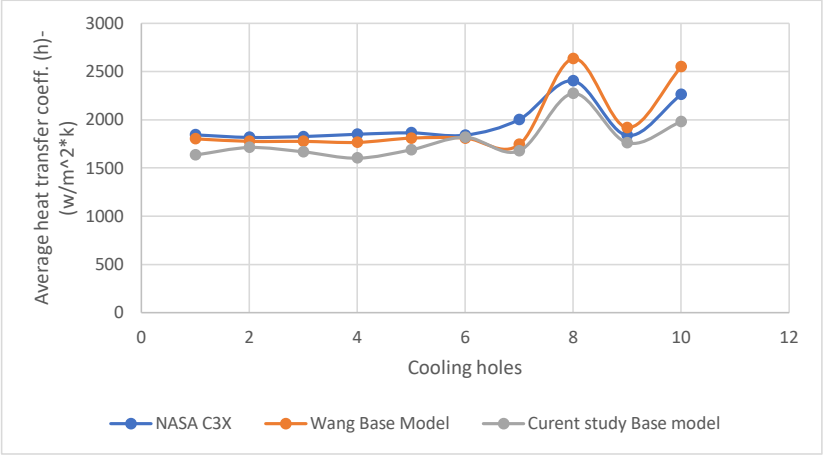

Fig. 4.13. Comparison of average heat transfer coefficient of NASA C3X experiment data, Wang experiment data, and current study's base model.

.

This section also delves deeper into the specifics of the cooling channels, noting their differences across various studies. A significant reduction in the hydraulic diameter of these channels (by approximately 59.70–69.55 %) is observed as they near the vane's trailing edge. This change is consequential for the performance of the cooling system and the heat transfer coefficients.

Additionally, the passage underscores differences in HTC values among various studies. These variations range from 2.9–15% between Hylton's original C3X computed data and the current study's CFD baseline case. Moreover, a difference of 2.4–26% is noted between the current study's CFD baseline case and Wang's computed data regarding cooling channel heat transfer coefficients. These findings highlight the pivotal role of cooling channels near the vane's trailing edge in influencing the heat transfer coefficient. They also illustrate that the results of the current study's CFD model significantly differ from previous studies, particularly in how they model and understand the cooling channels' impact on heat transfer.

This study highlights key distinctions from previous research, notably the departure from the fully developed flow assumption. Unlike prior studies, this research does not presume that the flow within the cooling channels has attained a steady state, with constant velocity and temperature profiles throughout. Instead, it accounts for variations in Reynolds numbers across individual cooling channels, which can influence heat transfer coefficients.

The focus of this study is a comparative analysis of two different cooling configurations: the base model and the jet impingement type. The methodology involves calculating the average heat transfer coefficient (HTC) for each cooling channel using a specific method or equation. The findings, as presented in Fig. 4.14, delineate the differences in average HTC for each cooling channel between

the two configurations. This comparative approach sheds light on the impact of the jet impingement-type configuration on the cooling efficiency of the channels and its comparative performance against the base model.

.

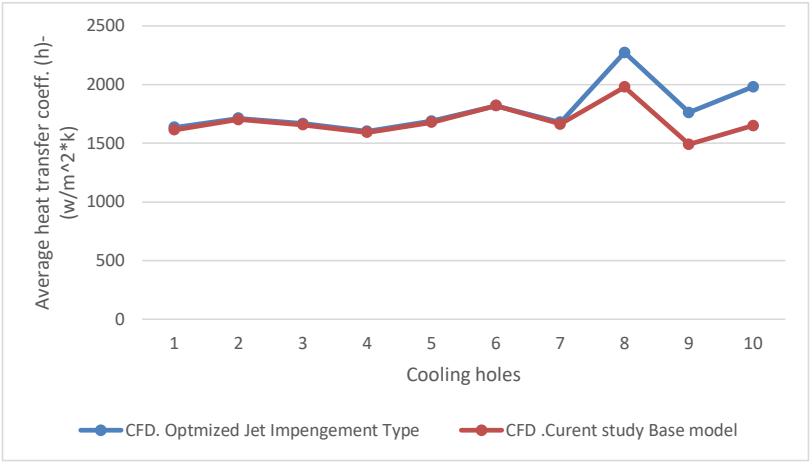

Fig. 4.14. Comparison of average heat transfer coefficient between current study base model and optimized jet impingement type.

Figure 4.15 reveals a minimal variance in the average HTC for the cooling holes between the base model and jet impingement-type configurations, with differences ranging from 0 % to 5 %. Despite expectations, channels 8/9/10, located in the jet impingement-type cooling channels, did not show significant differences. This outcome might be influenced by various factors, such as the cooling holes' geometry, the flow's Reynolds number, or the applied heat transfer model.

The comparative analysis helps understand how the jet impingement-type configuration influences cooling performance. It helps identify which channels exhibit the most notable differences in heat transfer coefficient between the two configurations. Additionally, Fig. 4.19 compares the blade wall heat flux between the NASA Base Model and the optimized model, further contributing to the study's comprehensive analysis of cooling configurations.

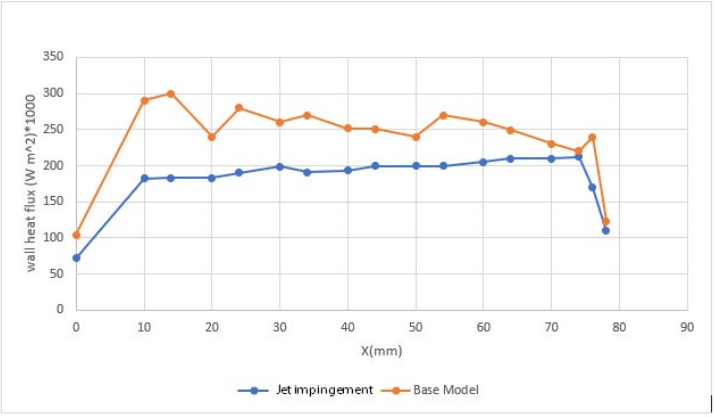

Fig. 4.15. Comparison of blade wall heat flux between base model and optimized model.

4.8.4. Determination of Cooling Effectiveness for the Optimized Model

Cunha mathematical formula is used to calculate the cooling effectiveness (φ) of a forced convection heat transfer system, such as a turbine blade cooling channel [29]. The equation considers the temperature difference between the coolant and the wall, the Reynolds number, and the Prandtl number. The general form of the Cunha equation is

$$\varphi = \frac{T_{gas} - T_{metal}}{T_{gas} - T_{c,in}}, \tag{4.20}$$

where

T_{gas} – the temperature of the gas in the fluid domain, K;

T_{metal} – the temperature of the solid, which is the blade in our study, K;

T_C, – the temperature of the coolant, which in our case is cold air, K.

By calculating the cooling effectiveness of a turbine blade with and without a triple impingement system, it is possible to compare the two systems and determine whether the optimized jet impingement system improves the cooling performance of the blade while minimizing losses to the overall turbine system. The cooling effectiveness values can be used as a metric to determine the improvement in cooling and can be used to optimize the design of the cooling system for maximum performance. By comparing the cooling effectiveness values of the two systems, engineers can determine the best design for the turbine blade cooling system and ensure that the blade operates within acceptable temperature limits, which is critical for the longevity and reliability of the turbine. The average coolant temperature is the inlet temperature for the cooling channels, the metal temperature as the temperature of the solid blade, and the gas temperature as the temperature of the hot fluid. These are commonly used inputs for calculating the cooling effectiveness. After calculating

the cooling effectiveness for the base model and optimized jet impingement model, we found it to be 0.4892 for the whole blade, and we compared it with the cooling effectiveness for the optimized jet impingement model, which is 0.6936. The results of the comparison between the base model and the optimized jet impingement model suggest that the optimized model has a significantly higher cooling effectiveness. The increase in cooling effectiveness of 29.46 % for the whole blade and 28.823 % for the trailing edge indicates that the optimized jet impingement design provides improved cooling performance. These results highlight the importance of considering optimized cooling designs for turbine blades to maintain efficient and safe operation.

GENERAL CONCLUSIONS

This Doctoral Thesis represents a substantial achievement in the field of aeronautical engineering, particularly in the design and analysis of cooling systems in gas turbine blades for civil aviation aircraft engines. The study covered several aspects for improved turbine blade cooling, such as improved cooling channel designs, numerical evaluation of heat and temperature variations in turbine blades, integration of MATLAB coding in assessing the heat transfer using computational fluid dynamics and optimized geometric configuration of jet impingement-type cooling channel for the enhanced cooling of the blade flow.

Key achievements of the Thesis include:

1. The evaluation of engine failures, particularly in the high-pressure turbine (HPT) section of CF6 engines installed on B747 aircraft, was conducted using EGT margins and BI data. This analysis provided the critical factors contributing to engine degradation and their impact on operational lifespan and maintenance costs.
2. In the CF6 engine study, a thorough examination of EGT margins provided valuable insights into engine performance deterioration. By analyzing a wide array of engine parameters, the study offered a view of the factors affecting engine health. This provided the basis for the cooling channel research.
3. From CFD analysis by utilizing ANSYS FLUENT and ANSYS ICEM, the research provided a detailed examination of various cooling channel configurations. This rigorous analysis has led to the identification of optimal designs of cooling channels with enhanced thermal performance and reduced drag, contributing significantly to overall turbine blade cooling.
4. MATLAB codes, which were developed specifically for the cooling channel thermal performance analysis, provided a significant way of comparing the simulated results (of the author) with the experimental data in the literature.
5. Jet impingement-type cooling channels were specifically designed for this Doctoral Thesis. The findings based on the Nusselt number ratio, Reynolds number effects, and thermal performance provide enhanced heat transfer effects within the blade channel.
6. This computational study compared the results of the designed cooling channels with the experimental results available in the literature for the NASA C3X turbine blade. This comparative analysis not only validates the results of previous studies but also provides new design methodologies for the cooling channels, leading to improved temperature profiles and profiles and heat transfer coefficients in turbine blades.
7. Even though the jet impingement cooling channels provide excellent means of heat transfer and blade cooling, there may be structural and manufacturing challenges to physically implement in the turbine blade. This limitation indeed does not affect the significance of the results achieved in this Thesis; however, in the future, this research can be continued for experimental analysis and to overcome the manufacturing constraints by the implementation of modern 3D printing-based additive manufacturing techniques.

REFERANCES

[1] Shirk, Willis L, "The Robert Barber, Jr. House: A Relic of Quaker Hegemony." *Journal of the Lancaster County Historical Society*; v. 96, no. 3,p ,1994.

[2] Tony Giampaolo, *Gas Turbine Handbook Principles and Practices*, 3rd Edition. The Fairmont Press, Inc., 2006.

[3] A. F. El-Sayed, *Aircraft Propulsion and Gas Turbine Engines, Second Edition*. CRC Press, 2017. doi: 10.1201/9781315156743.

[4] L. Gallar, C. Calcagni, V. Pachidis, and P. Pilidis, "Development of a One-Dimensional Dynamic Gas Turbine Secondary Air System Model – Part I: Tool Components Development and Validation," in *Volume 4: Cycle Innovations; Industrial and Cogeneration; Manufacturing Materials and Metallurgy; Marine*, ASMEDC, Jan. 2009, pp. 457–465. doi: 10.1115/GT2009-60058.

[5] H. Dai, J. Zhang, Y. Ren, N. Liu, and J. Lin, "Effect of cooling hole configurations on combustion and heat transfer in an aero-engine combustor," *Appl. Therm. Eng.*, vol. 182, p. 115664, Jan. 2021, doi: 10.1016/j.applthermaleng.2020.115664.

[6] R. S. Bunker, "Evolution of Turbine Cooling," in *Volume 1: Aircraft Engine; Fans and Blowers; Marine; Honors and Awards*, American Society of Mechanical Engineers, Jun. 2017. doi: 10.1115/GT2017-63205.

[7] P. H. Snyder and R.-R. North, "Seal Technology Development for Advanced Component for Airbreathing Engines," 2008. [Online]. Available: http://www.sti.nasa.gov

[8] J. Ji, D. Huang, B. Sun, S. Peng, and C. Pan, "Research on Active Control Strategy of Gas Turbine Secondary Air System in Different Ambient Temperature Conditions," in *Volume 5B: Heat Transfer*, American Society of Mechanical Engineers, Jun. 2017. doi: 10.1115/GT2017-63001.

[9] S. C. Pang, M. A. Kalam, H. H. Masjuki, and M. A. Hazrat, "A review on air flow and coolant flow circuit in vehicles' cooling system," *Int J Heat Mass Transf*, vol. 55, no. 23–24, pp. 6295–6306, Nov. 2012, doi: 10.1016/j.ijheatmasstransfer.2012.07.002.

[10] T. S. Chowdhury, F. T. Mohsin, M. M. Tonni, M. N. H. Mita, and M. M. Ehsan, "A critical review on gas turbine cooling performance and failure analysis of turbine blades," *International Journal of Thermofluids*, vol. 18, p. 100329, May 2023, doi: 10.1016/j.ijft.2023.100329.

[11] Waseem. Siddique, *Design of internal cooling passages investigation of thermal performance of serpentine passages*. Industrial Engineering and Management, Royal Institute of Technology, 2011.

[12] Logan E., *Handbook of Turbo Machinery*, 2nd ed. New York: CRC Press, 2003.

[13] J. A. Parsons and J. C. Han, "Rotation effect on jet impingement heat transfer in smooth rectangular channels with film coolant extraction," *International Journal of Rotating Machinery*, vol. 7, no. 2, pp. 87–103, 2001, doi: 10.1155/S1023621X01000082.

[14] L. D. Hylton and R. E. York, “Analytical and Experimental Evaluation of the Heat Transfer Distribution Over the Surfaces of Turbine Vanes,” 1983. Accessed: May 01, 1983. [Online]. Available: Analytical and Experimental Evaluation of the Heat Transfer Distribution Over the Surfaces of Turbine Vanes Hylton, York R.

[15] A. Ramadhan Al-Obaidi and I. Chaer, “Study of the flow characteristics, pressure drop and augmentation of heat performance in a horizontal pipe with and without twisted tape inserts,” *Case Studies in Thermal Engineering*, vol. 25, Jun. 2021, doi: 10.1016/j.csite.2021.100964.

[16] V. Nirmalan and L. D. Hylton, “An Experimental Study of Turbine Vane Heat Transfer with Leading Edge and Downstream Film Cooling,” in *Volume 4: Heat Transfer; Electric Power; Industrial and Cogeneration*, American Society of Mechanical Engineers, Jun. 1989. doi: 10.1115/89-GT-69.

[17] C. Glynn, T. O’Donovan, and D. Murray, “Jet Impingement Cooling,” *Proceedings of the 9th UK National Heat Transfer Conference*, Jan. 2005.

[18] Y. Yamane, Y. Ichikawa, M. Yamamoto, and S. Honami, “Effect of Injection Parameters on Jet Array Impingement Heat Transfer,” *International Journal of Gas Turbine, Propulsion and Power Systems*, vol. 4, no. 1, pp. 27–34, 2012, doi: 10.38036/jgpp.4.1_27.

[19] N. Mashoofi, S. Pourahmad, and S. M. Pesteei, “Study the effect of axially perforated twisted tapes on the thermal performance enhancement factor of a double tube heat exchanger,” *Case Studies in Thermal Engineering*, vol. 10, pp. 161–168, Sep. 2017, doi: 10.1016/j.csite.2017.06.001.

[20] G. O. Brown, “The History of the Darcy-Weisbach Equation for Pipe Flow Resistance,” in *Environmental and Water Resources History*, Reston, VA: American Society of Civil Engineers, Oct. 2002, pp. 34–43. doi: 10.1061/40650(2003)4.

[21] L. Wang, S. Wang, F. Wen, X. Zhou, and Z. Wang, “Heat transfer and flow characteristics of U-shaped cooling channels with novel wavy ribs under stationary and rotating conditions,” *Int. J. Heat Mass Transf.*, vol. 126, pp. 312–333, Nov. 2018, doi: 10.1016/j.ijheatmasstransfer.2018.05.123.

[22] J. Wang, B. Sundén, M. Zeng, and Q. Wang, “Film cooling effects on the tip flow characteristics of a gas turbine blade,” *Propulsion and Power Research*, vol. 4, no. 1, pp. 9–22, Mar. 2015, doi: 10.1016/j.jppr.2015.02.003.

[23] S.-F. Yang, H.-W. Wu, J.-C. Han, L. Zhang, and H.-K. Moon, “Heat transfer in a smooth rotating multi-passage channel with hub turning vane and trailing-edge slot ejection,” *Int. J. Heat Mass Transf.*, vol. 109, pp. 1–15, Jun. 2017, doi: 10.1016/j.ijheatmasstransfer.2017.01.059.

[24] M. Sajben, J. Kroutil, and C. Chen, “A high-speed schlieren investigation of diffuser flows with dynamic distortion,” in *13th Propulsion Conference*, Reston, Virgina: American Institute of Aeronautics and Astronautics, Jul. 1977. doi: 10.2514/6.1977-875.

[25] K. Wang, H. Li, and J. Zhu, “Experimental study of heat transfer characteristic on jet impingement cooling with film extraction flow,” *Appl. Therm. Eng.*, vol. 70, no. 1, pp. 620–

629, Sep. 2014, doi: 10.1016/j.applthermaleng.2014.05.077.
[26] A. J. Organ, “Counter-flow spiral heat exchanger – Spirex,” in *The Air Engine*, Elsevier, 2007, pp. 29–38. doi: 10.1533/9781845693602.1.29.
[27] “Fluent 6.2 Documentation File, ANSYS Manual, 2006”.
[28] C. D. Rossman, “Analysis of a Coupled Micro-and Triple-Impingement Cooling Analysis of a Coupled Micro-and Triple-Impingement Cooling Configuration in the C3X Vane Configuration in the C3X Vane.” [Online]. Available: https://commons.erau.edu/edt
[29] U. Uysal, P.-W. Li, M. K. Chyu, and F. J. Cunha, “Heat Transfer on Internal Surfaces of a Duct Subjected to Impingement of a Jet Array with Varying Jet Hole-Size and Spacing,” *J. Turbomach*, vol. 128, no. 1, pp. 158–165, Jan. 2006, doi: 10.1115/1.2101859.

Adham Ahmed Awad Elsayed Elmenshawy was born in 1986 in Belqas, Dakahlia, Egypt. He obtained his Bachelor's degree in Aviation Engineering from the Institute of Aviation Engineering and Technology, Egypt, in 2008 and a Master's degree in Aviation Transport from Riga Technical University in 2017. Since 2018, he has been a research assistant at Riga Technical University. He is currently a guest lecturer at the Transport and Telecommunication Institute, as well as an instructor at the APAC EASA Training Centre. He participated in exchange staff teaching within the Erasmus+ framework at Kaunas University of Applied Engineering Sciences (Lithuania) and has been involved in two European projects. He is a certified EASA Part 66/147 instructor. His research interests include fluid dynamics, aircraft engines, aircraft structures, robotics, material engineering, and UAVs.